Eindhoven University of Technology

MASTER

One dimensional DMOST and dual gate MOST analysis including velocity saturation effects

van de Wiel, P.J.A.M.

Award date:
1982

Link to publication

Disclaimer
This document contains a student thesis (bachelor's or master's), as authored by a student at Eindhoven University of Technology. Student theses are made available in the TU/e repository upon obtaining the required degree. The grade received is not published on the document as presented in the repository. The required complexity or quality of research of student theses may vary by program, and the required minimum study period may vary in duration.

General rights
Copyright and moral rights for the publications made accessible in the public portal are retained by the authors and/or other copyright owners and it is a condition of accessing publications that users recognise and abide by the legal requirements associated with these rights.

- Users may download and print one copy of any publication from the public portal for the purpose of private study or research.
- You may not further distribute the material or use it for any profit-making activity or commercial gain

4462

TECHNISCHE HOGESCHOOL EINDHOVEN

One Dimensional DMOST and Dual Gate MOST
Analysis including Velocity Saturation
Effects by P.J.A.M. van de Wiel.

EEA/300/10/1982

"De afdeling der Elektrotechniek van de
Technische Hogeschool Eindhoven aanvaardt
geen verantwoordelijkheid voor de inhoud
van stage- en afstudeerverslagen".

Verslag van het afstudeerwerk uitgevoerd
van 18-10-1981 tot 18-10-1982 op het
Philips Natuurkundig Laboratorium te
Eindhoven, o.l.v. Prof.dr.F.M.Klaassen.
Coach: Ir. L.J.M. Esser.

II

One Dimensional DMOST and Dual Gate MOST Analysis including Velocity Saturation Effects

Voorwoord

Dit verslag is het sluitstuk van mijn studie aan de Technische Hogeschool te Eindhoven. Het vormt een overzicht van mijn theoretische resultaten, die ik bij het verrichten van mijn afstudeeronderzoek, aan een nieuw type veld-effect transistor, op het Natuurkundig Laboratorium van Philips heb verkregen.
Verificatie van de theorie aan de praktijk is, tot nu toe alleen aan de hand van meetresultaten uit publicaties, verricht. De resultaten vertonen volledige kwalitatieve overeenkomsten, maar om de nauwkeurigheid van de formules te kunnen toetsen heb ik een chip ontworpen met teststructuren die zo goed mogelijk met het theoretisch model overeenkomen. De uitslag hiervan zal, in een publicatie verschijnen.
Mijn dank gaat vooral uit naar ir. L.J.M. Esser, die mij gedurende de afstudeerperiode uitstekend heeft begeleid, het onderwerp heeft geleverd en mij inzichten heeft verschaft, die uiteindelijk tot nieuwe resultaten hebben geleid.
Voorts gaat mijn erkentelijkheid uit naar prof.dr. F.M. Klaassen, die het mogelijk heeft gemaakt mijn afstudeerwerkzaamheden op het Nat.Lab. te kunnen verrichten en wiens kritische kanttekeningen op verschillende plaatsen in dit verslag tot verbetering hebben geleid. Ook ben ik dank verschuldigd aan ir. J. van Gils, bij wie ik bij het ontwerp van de chip met al mijn vragen van technologische aard terecht kon en die de chip uiteindelijk zal gaan maken en aan ing. J. van der Schoot die na de eerste theoretische resultaten, onmiddelijk handzame programma's heeft geschreven, waarmee de DMOST karakteristieken geplot konden worden.

Eindhoven, Oktober 1982 P.J.A.M. van de Wiel

Contents

1. Introduction 1

2. The MOS capacitor 3
 2.1. Introduction 3
 2.2. The ideal MOS curves 3
 2.3. The flat-band voltage 10

3. The MOS transistor 12
 3.1. Introduction 12
 3.2. Channel conductance 12
 3.3. Surface-space-charge region under nonequilibrium conditions 16
 3.4. Basic device characteristics 18
 3.5. Velocity saturation of electrons in silicon 25
 3.6. Device characteristics, adjusted for velocity saturation effects 28

4. The DMOST 33
 4.1. Introduction 33
 4.2. Operation modes of the DMOST 33
 4.3. The transition mode of the DMOST 38
 4.4. Basic device characteristics 41
 4.5. Conclusion 50

5. The depletion MOST 51
 5.1. Introduction 51
 5.2. Channel modes of a depletion MOST 52
 5.3. Bulk channel mode 53
 5.4. Twin channel mode 56
 5.5. Surface channel mode 58
 5.6. The basic device characteristics 59
 5.7. Derivation of the apparent threshold voltage V_{tA} 67
 5.8. The DMOST with N-surface layer 70
 5.9. Conclusion 72

6. The dual gate MOST 74
 6.1. Introduction 74
 6.2. Transconductance characteristics of the dual gate MOST 74
 6.3. Conclusion 78

References 79

Appendix A A1
Appendix B A3
Appendix C1 A4
Appendix C2 A5
Appendix D1 A6
Appendix D2 A8
Appendix E A9

1. Introduction

During the last years the DMOST has gained more attention owing to its high voltage properties and its improved linearity. In this thesis we will consider in particular the linearity aspects in terms of the transconductance.
A new one-dimensional analysis of the DMOST will be presented, where velocity saturation effects in both channel areas has been taken into account.
The results are closed form equations, however, they are rather laborious. Therefore, a set of approximated equations will be presented, which reduces the calculations considerably. Furthermore we will see that the equations hold for DMOSTs of the enhancement-enhancement type (both channel areas of P-type semiconductor) as well as for DMOSTs of the enhancement-depletion type (first channel area of P-type semiconductor and second channel area of N-type semiconductor). Finally, it will be shown that the equation set also can be applied to dual gate MOSTs.
In the next two chapters the electrical properties of an ordinary MOST are discussed in terms of channel charge and channel potential distributions. For derivation of the drain current only the main effects are considered. This will lead to an insight view, by which the operation of a DMOST can be understood.
Chapter 4 deals with the DMOST of the enhancement-enhancement type. Variations in the transconductance curves will be explained in terms of the device geometry and the doping concentrations.
In chapter 5 the properties of the depletion MOST are discussed. The results will be applied to the DMOST of the enhancement-depletion type.
In chapter 6 the dual gate MOST will be considered. Due to the two gates there are more bias conditions, which can be analysed with a little extension of the DMOST equation set.

The insights gained by this analysis can be used for adequate design to improve the linearity of the DMOST or dual gate MOST, as well as to derive the optimum biasing conditions.

2. The MOS capacitor

2.1. Introduction

In this chapter we will study the electrical properties of the Metal-Oxide-Semiconductor (MOS) system. The most often used semiconductor is silicon. Only the ideal MOS curves will be derived. For a more extensive treatment see Sze [1,pp. 425-40] .

2.2. The ideal MOS curves

The MOS system is formed by a metal gate on an oxidized silicon wafer (see fig. 2.1.).

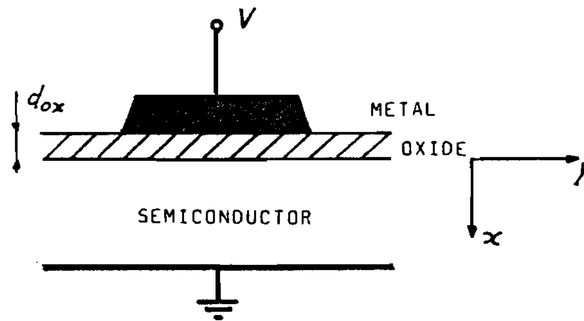

Fig. 2.1. Metal-oxide semiconductor (MOS) structure.

V_g is the applied voltage on the gate and is positive when the gate is positively biased with respect to the ohmic contact, which is assumed to be on ground potential. Only P-type silicon will be treated. The properties of N-type silicon follow in the same manner by replacing electrons by holes and v.v. and inverting the potential on the gate.

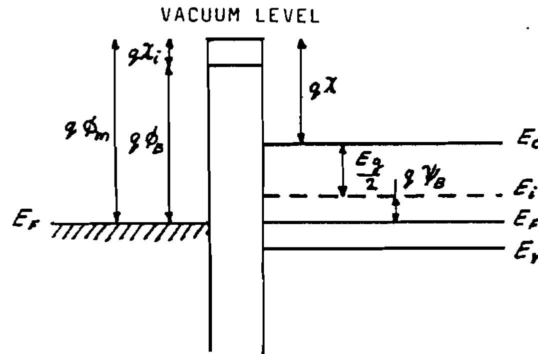

Fig. 2.2. Energy band diagram for the ideal MOS structure at V_g=0.

Fig. 2.2. shows the energy level diagram of an ideal MOS structure for V_g=0V. Here is Øm the metal work function χ the semiconductor electron affinity, χ_i the insulator electron affinity. E_g the band gap, E_V the top energy level of the valence band, E_C the bottom energy level of the conduction band, $\emptyset_B$ the potential barrier between the metal and the insulator, and ψ_B the potential difference between the Fermi level E_F and the intrinsic level E_i. The ideal MOS capacitor is defined as follows:

1) At zero applied bias there is no energy difference between the metal workfunction Øm and the semiconductor workfunction Øs, with

$$\phi_s = \chi + \frac{E_g}{2q} + \psi_B$$

   This means that the workfunction difference Øms is zero.
2) The only charges in the structure are those in the semiconductor and those with equal number but opposite sign on the metal surface adjacent to the oxide.
3) The resistivity of the oxide is infinite.

We can distinguish three cases which may exist at the semiconductor surface under biasing conditions (see fig. 2.3.).

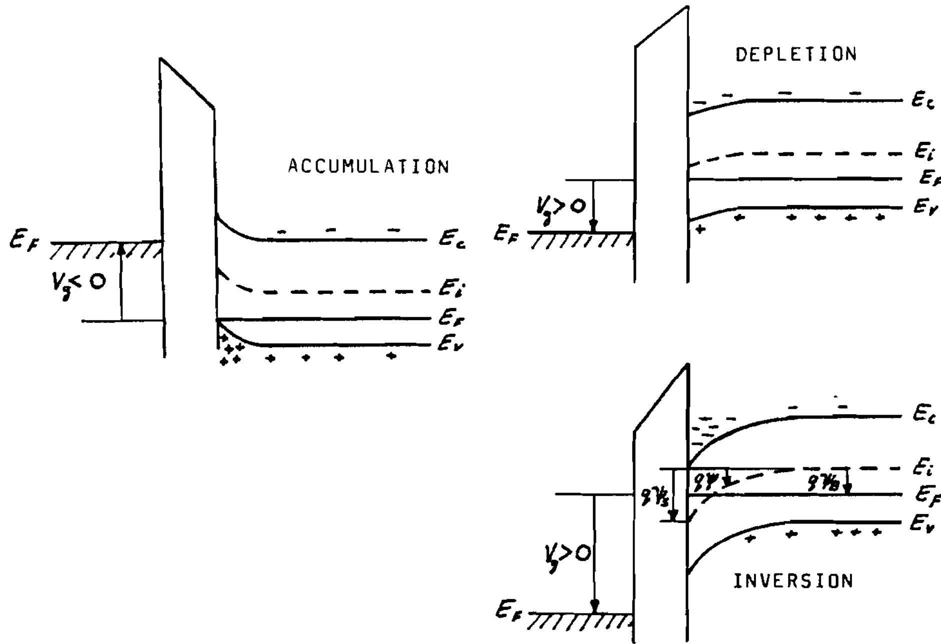

Fig. 2.3. Energy band diagrams for the ideal MOS structure with P-type semiconductor when $V\neq0$.

When a negative voltage ($V_g<0$) is applied to the metal gate the top of the intrinsic level bends upward and is further away from the Fermi level. Since the carrier density depends exponentially on the energy difference (E_i-E_F), this band bending causes an accumulation of majority carriers (holes) near the semiconductor surface. This is the case of "accumulation". When a small positive voltage ($V_g>0$) is applied, the bands bend downward, and the majority carriers are depleted. This is the case of "depletion". When a larger positive voltage is applied, the bands bend even more downward such that the intrinsic level E_i at the surface crosses the Fermi level E_F. At this point the number of electrons at the surface is larger than that of the holes, the surface is inverted, and this is the case of "inversion".
The electrostatic potential ψ (see fig. 2.3.) is defined as zero in the bulk of the silicon, and is measured with respect to the intrinsic level in the bulk. At the semiconductor surface $\psi=\psi_s$ and ψ_s is called the surface potential. Though

the carriers in the semiconductor are distributed as an exponential function of ψ , the accumulation charge as well as the inversion charge is considered to be in an infinitesimal layer at the semiconductor surface. Furthermore, we will use Shockleys depletion-layer approximation, i.e. there are no free carriers in the depleted region and outside this region the semiconductor is assumed to be neutral. This results in a space charge region for the depleted region.

In either the three cases we can derive the potential distribution in the structure.

For $V_g<0$, all accumulation charge is assumed to be at the surface, so the whole semiconductor is neutral. This implies that the whole potential appears across the oxide. The accumulation charge as well as the gate charge follows by

$$Q_{acc} = - Q_g = - C_{ox} V_g = - \frac{\varepsilon_{ox}}{d_{ox}} V_g \qquad [2.1.]$$

where Q_{acc} is the accumulation charge per unit area, Q_g is the charge in the gate per unit area, C_{ox} is the capacitance per unit area, ε_{ox} the permitivity and d_{ox} the thickness of the oxide.

If $V_g>0$, a depletion layer will be formed in the silicon (see fig. 2.4.).

The electric field and potential distribution follow simply by solving the one dimensional Poisson equation.

$$\frac{\partial^2 \psi}{\partial x^2} = - \frac{\rho(x)}{\varepsilon}$$

The semiconductor is uniformly doped so $\rho(x) = q N_A$ in the depleted area with N_A the doping concentration of the silicon, and $\rho(x)=0$ in the oxide and in the semiconductor outside the depleted area. The depletion charge as well as the induced charge in the gate is given by

$$Q_g = - Q_{depl} = C_{ox} (V_g - \psi_s) \qquad [2.2.]$$

On the other hand the depletion charge is related to ψ_s by

$$Q_{depl} = -qN_A d = -\sqrt{2\varepsilon_s q N_A \psi_s} \qquad [2.3.]$$

where d is the width of the depleted region.

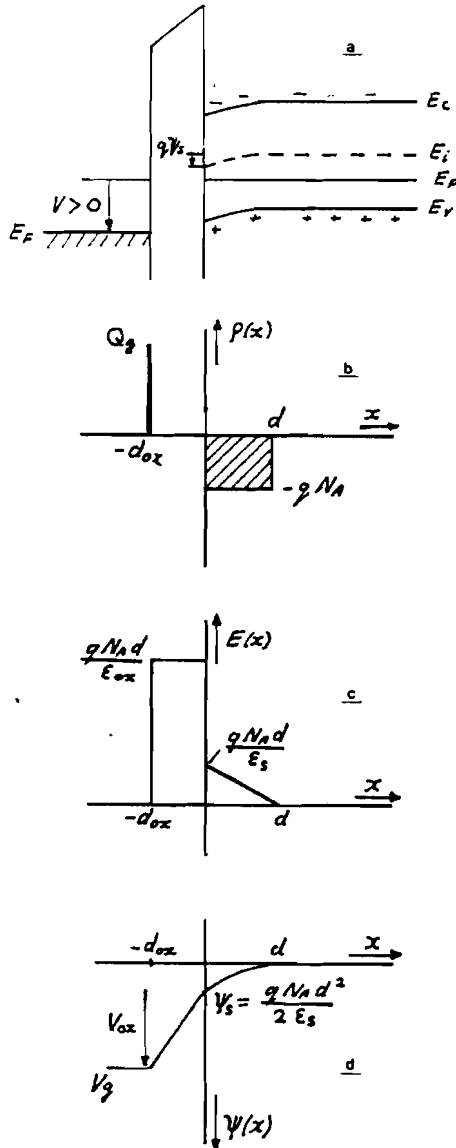

Fig. 2.4. The ideal MOS structure under depletion conditions.
a. Band diagram
b. Charge distribution
c. Electric field distribution
d. Potential distribution

By increasing V_g inversion occurs. Strong inversion starts when $\psi_s = 2\psi_B$. In this situation the electron concentration at the surface equals the hole concentration in the neutral part of the semiconductor. ψ_s by inversion is given by

$$\psi_s(inv) = 2\psi_B = \frac{2kT}{q} \ln \frac{N_A}{n_i} \qquad [2.4.]$$

where k is the Boltzman factor, T the absolute temperature and n_i the intrinsic carrier concentration of the semiconductor. The depletion width in this situation is

$$d_p = \sqrt{\frac{2\varepsilon_s(2\psi_B)}{qN_A}} \qquad [2.5.]$$

and can be solved by substituting Eq. [2.4] into Eq. [2.5.]. By further increase of Vg the number of minorities (electrons) increases enormously, so the depletion charges hardly influence the charge balance. The depletion depth remains almost constant and is assumed to be d_p (see fig. 2.5.).

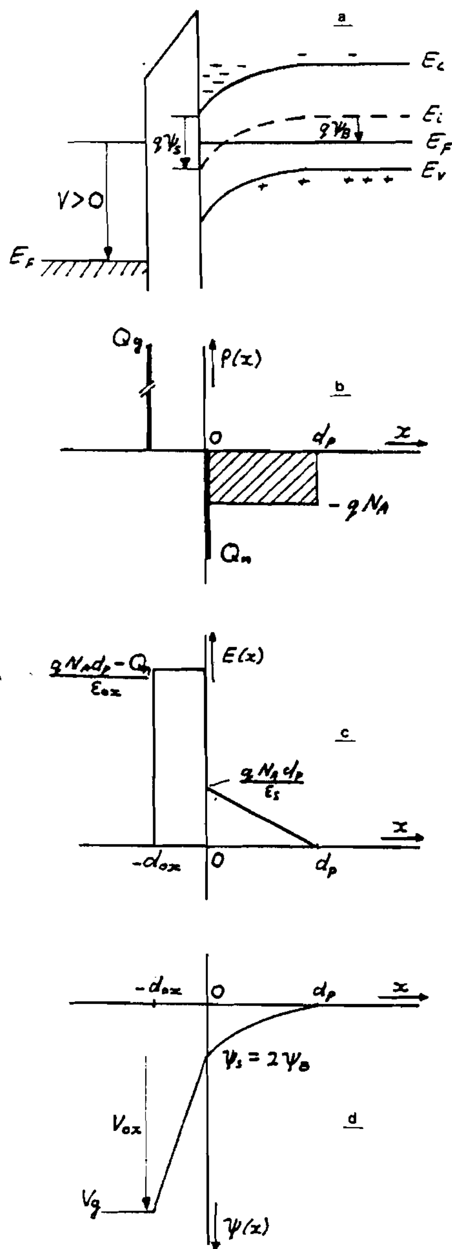

Fig. 2.5. The ideal MOS structure under inversion conditions
a. Band diagram
b. Charge distribution
c. Electric field distribution
d. Potential distribution

Because the inversion layer is infinitesimal thin, the surface potential remains constant by increasing V_g under inversion conditions, as can be seen by rewriting Eq. [2.5] :

$$\psi_s(inv) = 2\psi_B = \frac{q N_A d_p^2}{2\varepsilon_s} \qquad [2.6.]$$

The inversion charge per unit area Q_n follows by the voltage across the oxide with the capacitance formula

$$V_g - 2\psi_B = \frac{-Q_n + q N_A d_p}{C_{ox}} \qquad [2.7.]$$

$$= -\frac{Q_n}{C_{ox}} + V'_{ox} \qquad [2.8.]$$

with $$V'_{ox} = \frac{q N_A d_p}{C_{ox}} \qquad [2.9]$$

V'_{ox} is a constant part of the voltage across the oxide which is caused by the depletion charge. The gate voltage at which strong inversion starts is a quantity of interest. It is called the turn-on voltage V_t.
This voltage follows from Eq. [2.7] by setting Q_n to zero.

$$V_g = V_t = 2\psi_B + \frac{q N_A d_p}{C_{ox}}$$
$$= 2\psi_B + V'_{ox}$$
$$= 2\psi_B + \sqrt{2\varepsilon_s q N_A (2\psi_B)} \qquad [2.10.]$$

Substitution of Eq. [2.10] into Eq. [2.8] yields

$$|Q_n| = C_{ox}(V_g - V_t) \qquad [2.11.]$$

We can see that the channel charge is proportional to V_g.

It is usefull to consider the potential distribution at inversion over the length of the MOS structure, i.e. in the y-direction (see fig. 2.6.).

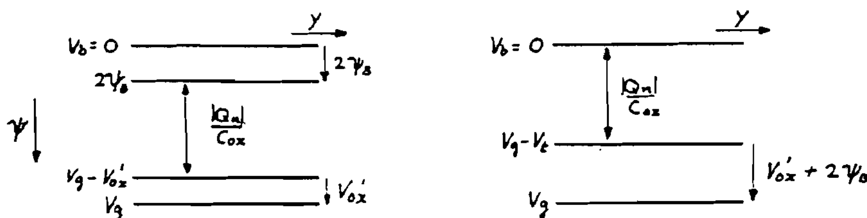

Fig. 2.6. Potential distribution along the y-axis. In the right-hand figure the turn-on voltage V_t is introduced.

As shown in fig. 2.6b the inversion charge is proportional to the distance between the curves $V=0$ and $V=V_g-V_t$.

2.3. The flat-band voltage

In this subsection two non-ideal properties will be treated. First we will consider the situation with a workfunction difference between metal and silicon and second we will take surface charges into account.
Fig. 2.7. shows the energy-level diagram of the metal, oxide and semiconductor before and after contact.

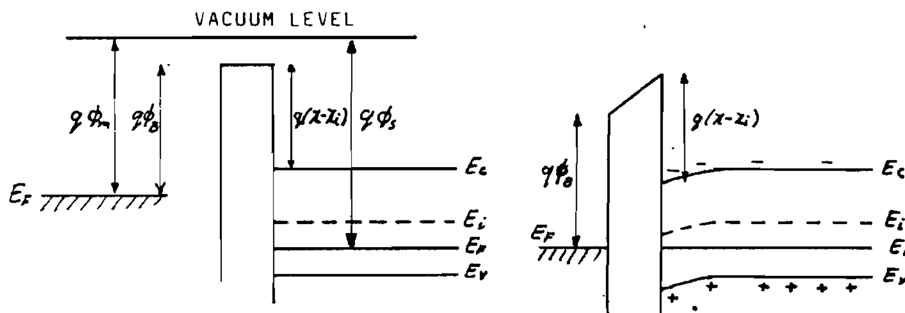

Fig. 2.7. Energy-level diagram of the metal, oxide and semiconductor before and after contact.

After contact a redistribution of charges occurs and the equilibrium condition is reached when the Fermi levels of the metal and the semiconductor are at equal heights. Owing to the redistribution of charge the bands in the semiconductor are bent. These bands can be flattened by applying a gate voltage equal to $\emptyset_{ms}$.
The surface charge is caused by oxidizing the silicon. This surface charge is fixed and cannot be changed due to a variation of ψ_s. The effect of the fixed charges to the potential distribution is equal to an applied gate voltage of

$$V_g = \frac{Q_s}{C_{ox}}$$

where Q_s is the fixed surface charge per unit area. So this surface charge also delivers a band bending. To eliminate the band bending caused by the surface charge

and workfunction difference a gate voltage of

$$V_g(\text{flat-band}) = \phi_{ms} - \frac{Q_s}{C_{ox}} = V_{FB}$$

is needed, where V_{FB} is called the flat-band voltage.
It is handy to take the flat-band situation as a reference and reduce all gate voltages with V_{FB}.
In this thesis we assume that all gate voltages are reduced with V_{FB} without mentioning this explicitely.

3. The MOS transistor

3.1. Introduction

The metal-oxide-semiconductor transistor (MOST) belongs to the class of field effect transistors. The basic device characteristics will be derived and will be explained in terms of channel charges and channel potentials. In the last subsection velocity saturation of the electrons will be taken into account.

3.2. Channel conductance

The basic structure of a MOST is illustrated in fig. 3.1. This device consists of a P^--type silicon substrate into which two N^+ regions, the source and the drain, are formed (e.g. by diffusion or by ion-implantation). The metal contact on the oxide is called the gate electrode.

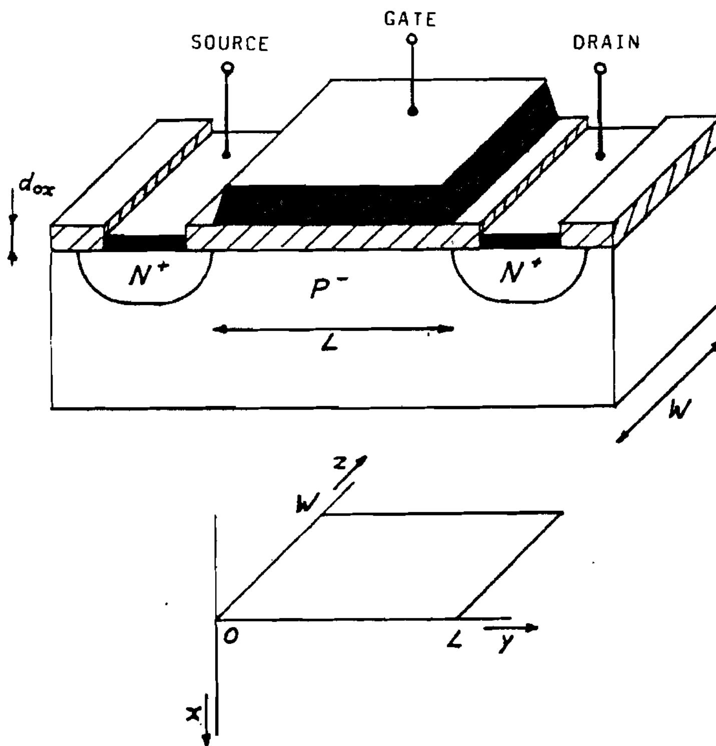

Fig. 3.1. Schematic diagram of a MOST.

When there is no voltage applied to the gate, the source-to-drain electrodes correspond to two p-n junctions connected back to back. The only current that can flow from the drain to the source is the reverse leakage current. When a sufficiently large positive bias is applied to the gate, a surface inversion layer is formed between the two N^+ regions.
The source and the drain are thus connected by a conducting surface channel through which a large current can flow. The conductance of this channel can be modulated by varying the gate voltage. If a voltage between drain and source is applied a current will flow which varies with varying channel conductance. Before deriving this current, we must consider the p-n junction between bulk and source at zero source voltage V_s. Fig. 3.2. shows the energy level diagram at the semi-conductor surface if no gate voltage is applied and the bulk potential V_b=0.

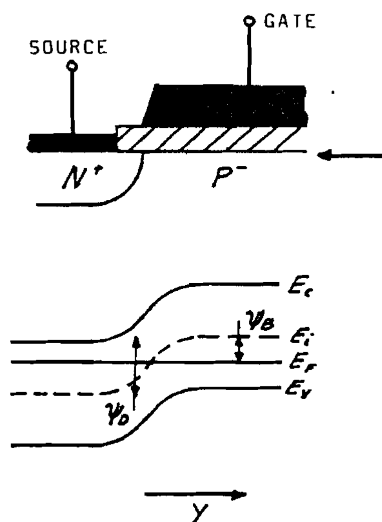

Fig. 3.2. Energy-level diagram along the y-axis at the semi-conductor surface for V_g=0.

In this figure ψ_o is the built-in voltage

$$\psi_o = \frac{kT}{q} \ln \frac{N_A N_D}{n_i^2} \qquad [3.1]$$

where N_D is the donor concentration of the N^+ region .
Next consider the energy level diagram for $V_g > V_t$, so the

surface of the P-region is inverted (see fig. 3.3.a).

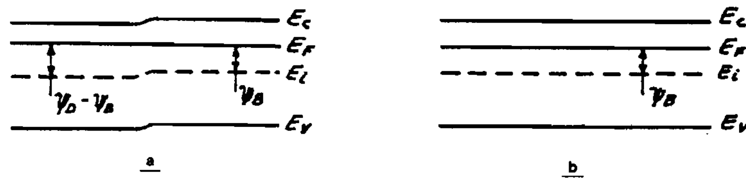

Fig. 3.3. Energy-level diagram along the y-axis at the semiconductor surface for $V_g > V_t$ with
a. $\psi_D > 2\psi_B$
b. $\psi_D = 2\psi_B$

Notice $2\psi_B = \psi_D$ only if the donor concentration in the source equals the acceptor concentration in the bulk.
We will use this equality although the donor concentration exceeds the acceptor concentration. This results in flat bands for E_i, E_V and E_c in fig. 3.3.b. At the drain side the same conditions hold.
In order to show more clearly the band bending in the bulk, the MOST in Fig. 3.1. is turned 90 degreeds and is shown in Fig. 3.4.a. In fig. 3.4.b. and fig. 3.4.c. the Fermi level (solid lines) and intrinsic level (dashed lines) are shown for $V_g=0$ and $V_g>V_t$ respectively, and $V_d=V_s=V_b=0$.
The chain-dotted line indicates where E_i crosses E_F.
Because the structure will be considered under non-equilibrium conditions we will take the source potential as reference and all potentials will be taken with respect to the source, i.e. $V_g=V_{gs}$, $V_b=V_{bs}$, etc.

If we apply a negative bulk voltage (V_b) under inversion conditions by keeping the drain and source potential to zero, the depletion region will grow because holes are extracted (see fig. 3.5.).

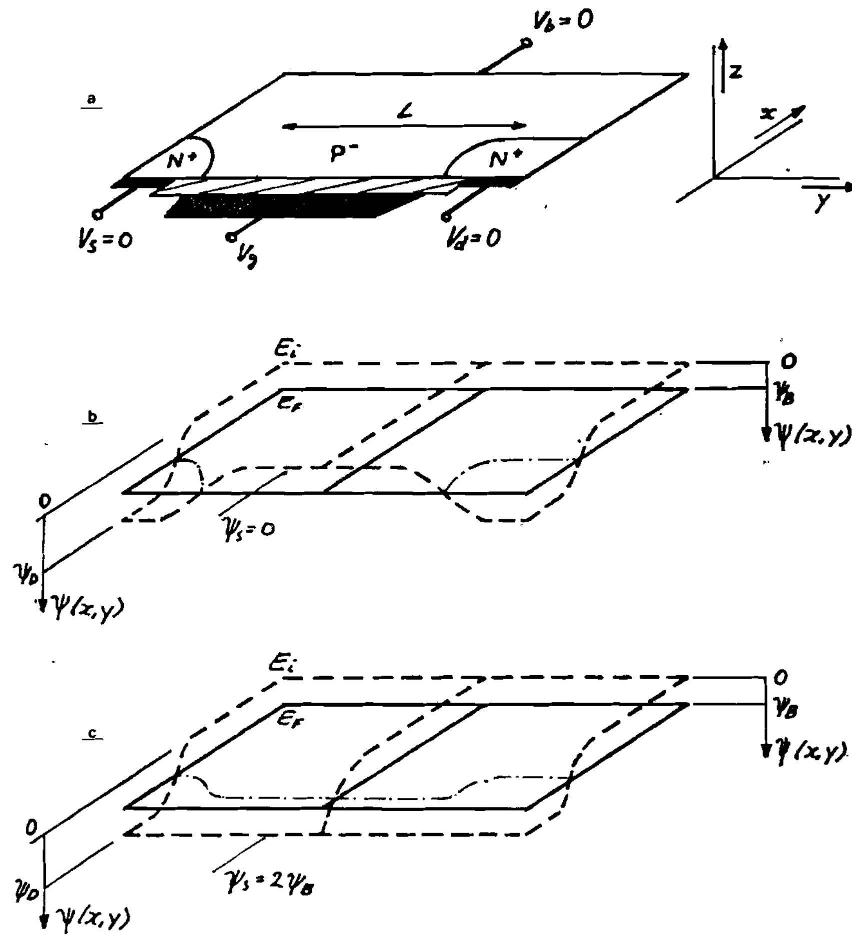

Fig. 3.4. a. The MOST structure from Fig. 3.1., turned over 90 degrees.
b. Two dimensional diagram of the Fermi level (solid lines) and the intrinsic level (dashed lines) at zero volts gate bias.
c. Two dimensional diagram of the Fermi level and intrinsic level for $V_g > V_t$.

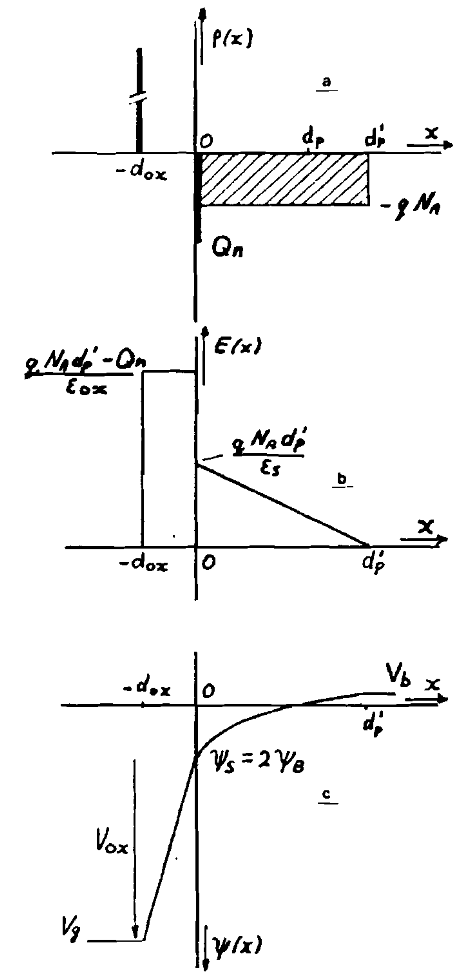

Fig. 3.5. The MOST under inversion conditions with negative applied bulk bias.
a. Charge distribution
b. Electric field distribution
c. Potential distribution.

By the fact of the well conducting channel while the drain and source are grounded, the surface potential remains $2\psi_B$. The electrostatic potential across the oxide remains $V_g - 2\psi_B$ thus the total charge remains constant. This means that at a decrease of the negative bulk voltage the channel charges are diminished with the same amount at which the depletion charge is increased.
The depletion charge per unit area is given by

$$Q_{depl} = -q N_A d_p' = -\sqrt{2 \varepsilon_s q N_A (2\psi_B - V_b)} \qquad [3.2.]$$

If a positive drainvoltage is applied, channel electrons are drawn towards the drain.
Just as in the previous situation (V_b<0) this results in an enlarged depletion region. Under these conditions no longer thermal equilibrium exists, so first, we will consider the MOS structure under nonequilibrium conditions.

3.3. Surface-space-charge region under nonequilibrium conditions

If a voltage is applied across the drain-source contacts, the imref (quasi Fermi level) of the minority carriers (electrons) is lowered from the equilibrium Fermi level. There is a variation of the band in the y direction due to the applied reverse bias on the drain. An inversion layer can be formed only when the potential at the surface crosses the imref of the electrons. Fig. 3.6. shows a comparison of the charge distribution and energy band variation of an inverted P region for (a) the equilibrium case and (b) the nonequilibrium case at the drain.

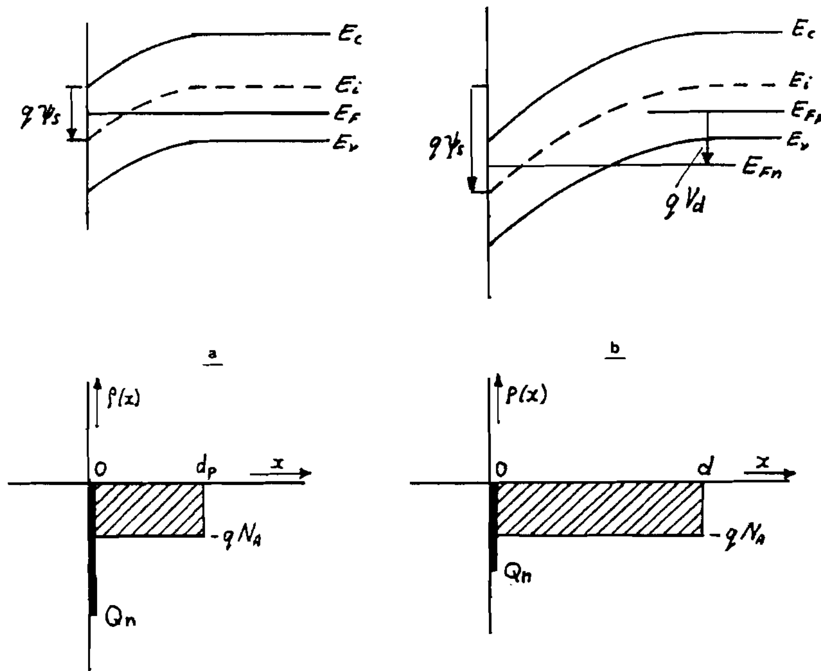

Fig. 3.6. Comparison of the charge distribution and energy band variation of an inverted P-region for
a. the equilibrium case and
b. the nonequilibrium case at the drain.

In the nonequilibrium case the hole concentration is hardly affected, so the imref for holes E_{Fp} of the silicon does not vary with the distance from the bulk to the surface. The imref for the electrons E_{Fn} of silicon is separated by the applied junction bias V_d from the imref of holes i.e.

$$E_{Fp} = E_{Fn} - qV_d$$

It follows for the inversion condition that

$$\psi_s(inv) = V_d + 2\psi_B \qquad [3.3]$$

Fig. 3.7. shows the band bending in a cross section of the MOST.

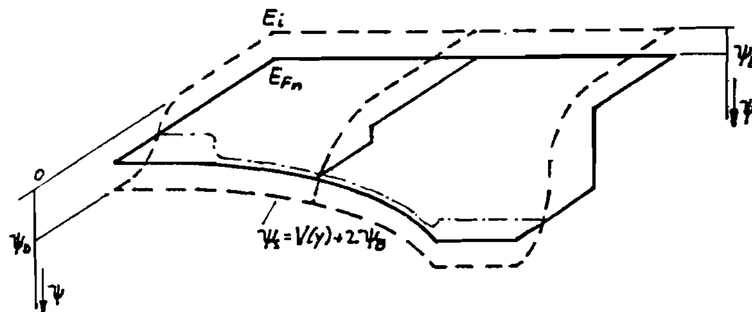

Fig. 3.7. Two dimensional diagram of the imref for electrons (solid lines) and the intrinsic level (dashed lines) for a MOST under nonquilibrium conditions.

3.4. Basic device characteristics

The conductivity of the channel can be approximated by (n>>p)

$$\sigma(y) = q\, n(y)\, \mu_n \qquad [3.4.]$$

where n is the electron density per unit area, p is the hole density per unit area, μ_n is the mobility of electrons which is assumed to be constant. To derive the drain current we will use the so-called gradual channel approximation i.e. the transversal field (E_x in x direction) in the channel is much larger than the longitudinal field (E_y in y direction).

The charge in the inversion layer follows with (see fig. 3.8.).

$$V_{ox} = V_g - \psi_s(y) = \frac{-Q_n(y) + q N_A d(y)}{C_{ox}} \qquad [3.5.]$$

$$V_g - V'_{ox}(y) - \psi_s(y) = -\frac{Q_n(y)}{C_{ox}} \qquad [3.6.]$$

$$\text{with} \quad V'_{ox}(y) = \frac{q N_A d(y)}{C_{ox}} \qquad [3.7.]$$

The surface potential $\psi_s(y)$ at inversion is approximated by $2\psi_B + V(y)$ where V(y) is the potential difference between the point y and the source electrode.

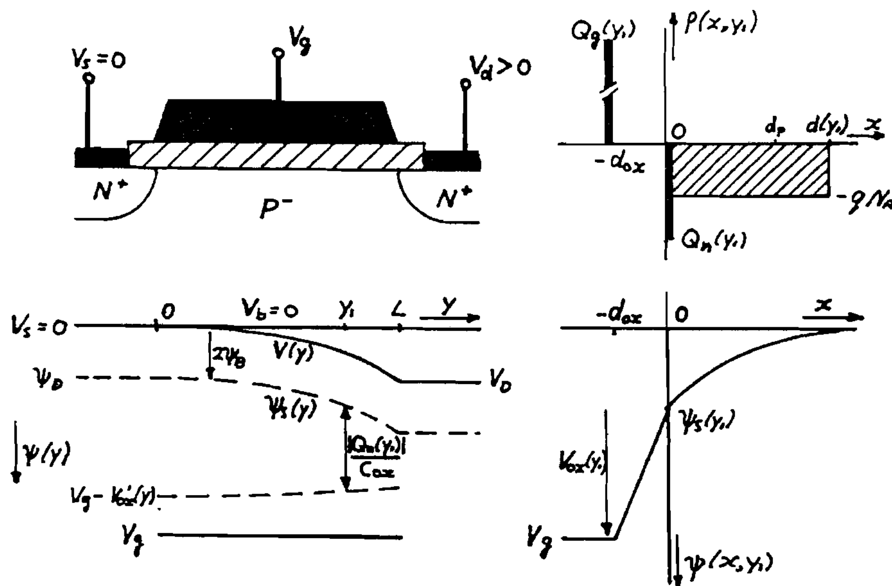

Fig. 3.8. The MOST under nonequilibrium conditions
a. Longitudinal potential distribution (y direction)
b. Transversal potential distribution (x direction at $y=y_1$) with corresponding charge distribution.

As can be seen with Eq. [3.6] the distance between $\psi_s(y)$ and $V_g - V'_{ox}(y)$ is proportional to the channel charge.
The local depletion depth $d(y)$ is given by

$$d(y) = \sqrt{\frac{2\varepsilon_s\,(V(y) + 2\psi_B)}{q N_A}} \qquad [3.8]$$

Substitution of Eq[3.8] into Eq. [3.5] yields

$$Q_n(y) = -[V_g - 2\psi_B - V(y)]\,C_{ox} + \sqrt{2\varepsilon_s q N_A\,(V(y) + 2\psi_B)} \qquad [3.9]$$

The channel resistance of an elementary section (dy) is given by

$$dR = \frac{dy}{W\mu_n\,|Q_n(y)|} \qquad [3.10]$$

Where W is the total width of the MOST. (see fig. 3.1.).
And the voltage drop across this elementary section is given by

$$dV(y) = I_d\,dR = \frac{I_d\,dy}{W\mu_n\,|Q_n(y)|} \qquad [3.11]$$

where I_d is the draincurrent which is a constant, independent of y. Substitution of Eq.[3.9] into Eq. [3.11] and integration from the source (y=0, V=0) to the drain (y=L, $V=V_d$) yields(see appendix A).

$$I_d = \frac{W\mu_n C_{ox}}{L}\left\{\left(V_g - 2\psi_B - \frac{V_d}{2}\right)V_d - \frac{2}{3}\frac{\sqrt{2\varepsilon_s q N_A}}{C_{ox}}\left[(V_d + 2\psi_B)^{3/2} - (2\psi_B)^{3/2}\right]\right\} \qquad [3.12]$$

If a negative bulk voltage is applied, the local depletion width is

$$d(y) = \sqrt{\frac{2\varepsilon_s\,(V(y) + 2\psi_B - V_b)}{q N_A}} \qquad [3.13]$$

which leads to

$$I_d = \frac{W\mu_n C_{ox}}{L}\left\{\left(V_g - 2\psi_B - \frac{V_d}{2}\right)V_d - \frac{2}{3}\frac{\sqrt{2\varepsilon_s q N_A}}{C_{ox}}\left[(V_d + 2\psi_B - V_b)^{3/2} - (2\psi_B - V_b)^{3/2}\right]\right\} \qquad [3.14]$$

for the drain current.
Eq. [3.14] can be approximated for small V_d by

$$I_d = \beta\left[(V_g - V_t)V_d - \frac{V_d^2}{2}\right] \qquad [3.15]$$

if only two terms of the Taylor expansion of $(V_d + 2\psi_B - V_b)^{3/2}$

are taken into account and

$$I_d = \beta\left[(V_g - V_t)V_d - (1+\delta)\frac{V_d^2}{2}\right] \qquad [3.16]$$

if three terms are taken into account.

In these equations the following constants are defined

$$\beta = \frac{W \mu_n C_{ox}}{L} \qquad [3.17]$$

$$V_t = 2\psi_B + K_p\sqrt{2\psi_B - V_b} \qquad [3.18]$$

$$\delta = \frac{K_p}{2\sqrt{2\psi_B - V_b}} \qquad [3.19]$$

$$K_p = \frac{\sqrt{2\varepsilon_s q N_A}}{C_{ox}} \qquad [3.20]$$

where K_p is called the bulk factor.

It should be noticed that Eq. [3.18] results in Eq. [2.10] if $V_b=0$. The basic device characteristics will be explained by using Eq. [3.15] . Because this is an approximated formula it does not agree with the potential distribution shown in fig. 3.8. Fig. 3.9. shows the potential distribution which agrees with Eq.[3.15.]

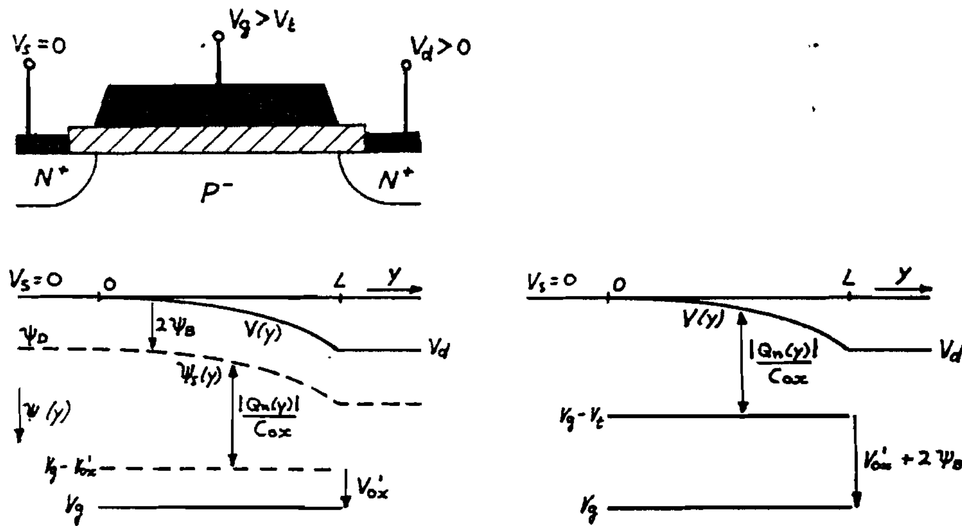

Fig. 3.9. Approximated potential distribution along the y-axis for a MOST under nonequilibrium conditions (see text). In the right-hand figure the threshold voltage V_t is introduced.

It can be shown (see appendix B) that the approximation results in a constant depletion width. This depletion width is equal to the one in the situation with drain and source grounded. The potential V'_{ox} is then also constant and given by

$$V'_{ox} = \frac{\sqrt{2\varepsilon_s q N_A (2\psi_B - V_b)}}{C_{ox}} = K_p\sqrt{2\psi_B - V_b} \qquad [3.21]$$

In fig. 3.9. the distance between V(y) and $V_g - V_t$ is proportional to the channel charge. Substitution of Eq. [3.21] into Eq . [3.6] yields

$$Q_n(y) = -[V_g - 2\psi_B - V(y)]C_{ox} + \sqrt{2\varepsilon_s q N_A (2\psi_B - V_b)} = -[V_g - V_t - V(y)]C_{ox} \qquad [3.22]$$

Starting with the situation of fig. 3.9. we can increase V_g by constant V_d. It follows immediately that the channel charge increases linearly with $V_g - V_t$, so the drain current increases linearly with $V_g - V_t$. This agrees with Eq. [3.15]. This operation mode of the MOST is called the linear or triode region.

Due to the parabolic channel charge distribution(this will be proved in the next subsection), the drain current depends quadratically to the drain voltage. This also agrees with Eq. [3.5].

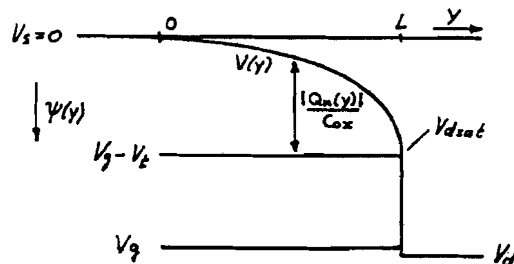

Fig. 3.10. Longitudinal potential distribution of a MOST which operates in the saturation region.

When the drain voltage is increased to a point such that the channel charge at y=L becomes zero, the number of mobile electrons at the drain shows a drastic fall-off. The drain voltage and the drain current at this point, called

the pinch off point, are designated as V_{dsat} and I_{dsat} respectively. The value of V_{dsat} is obtained from Eq. [3.22.] under the conditions $V(L) = V_{dsat}$ and $Q_n(L)=0$.

$$V_{dsat} = V_g - V_t \qquad [3.23.]$$

This condition is shown in fig. 3.10. When $V_d \geqslant V_{dsat}$ we have the saturation or pentode region.
Substitution of Eq. [3.23] into Eq. [3.15] yields

$$I_{dsat} = \beta \frac{(V_g - V_t)^2}{2} = \beta \frac{V_{dsat}^2}{2} \qquad [3.24]$$

The drain current is independent of the drain voltage in the pentode region, because all extra drain voltage appears beyond the pinch off point.
When we apply a drainvoltage beyond the saturation drain-voltage, we can increase the gate voltage while the MOST remains in pentode region (see fig. 3.11). In this situation the channel charge as well as the potential across the channel increases, with increasing gate voltage.

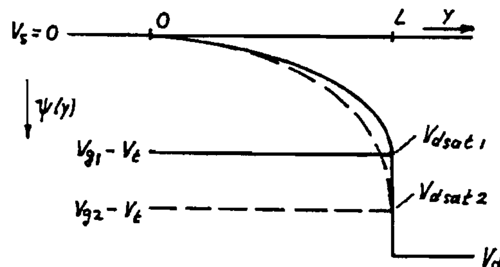

Fig. 3.11. Comparison of the longitudinal potential distribution for two different values of the gate voltage, with $V_{g2} > V_{g1}$, for a MOST which operates in the pentode region.

The drain current is fully quadratic related to the potential across the channel. This potential is equal to $V_g - V_t$, so $I_d \backsim (V_{dsat})^2 \backsim (V_g - V_t)^2$.
The output characteristics of the MOST, described with Eq. [3.15], are shown in Fig. 3.12. The dotted line indicates the locus of the drain voltage (V_{dsat}) at which the

current reaches a maximum value.

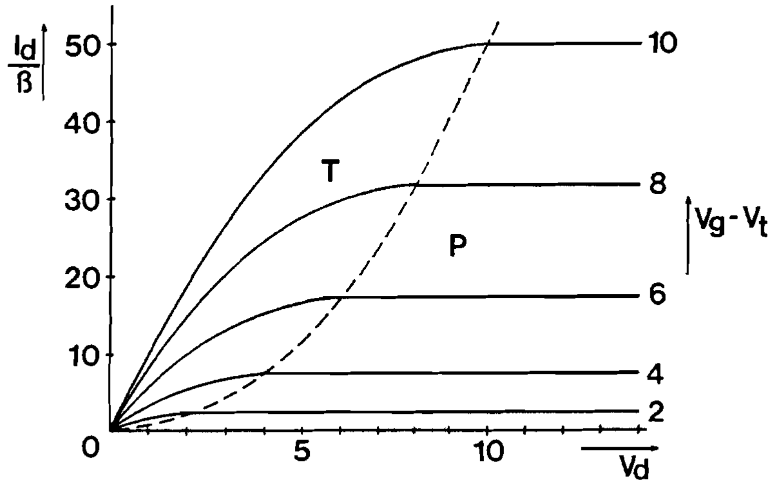

Fig. 3.12. Drain current vs drain voltage with the gate voltage as parameter. The triode and pentode region are indicated by T and P respectively.

The triode and pentode region are indicated by T and P respectively. As can be seen immediately, the drain current is independent of the drian voltage in the pentode region and proportional to the second power of $V_g - V_t$. In the triode region the draincurrent increases linearly with increasing V_g at constant V_d.

The transconductance g_m is given as

$$g_m = \frac{\partial I_d}{\partial V_g}\bigg|_{V_d = const} = \beta V_d \qquad [3.25.]$$

for triode region and

$$g_{msat} = \beta (V_g - V_t) \qquad [3.26.]$$

for the pentode region. The intercepts of the V_g=const. lines in fig. 3.12 are proportional to the transconductance.

Figure 3.13. shows the transconductance versus the gate voltage with the drain voltage as parameter.

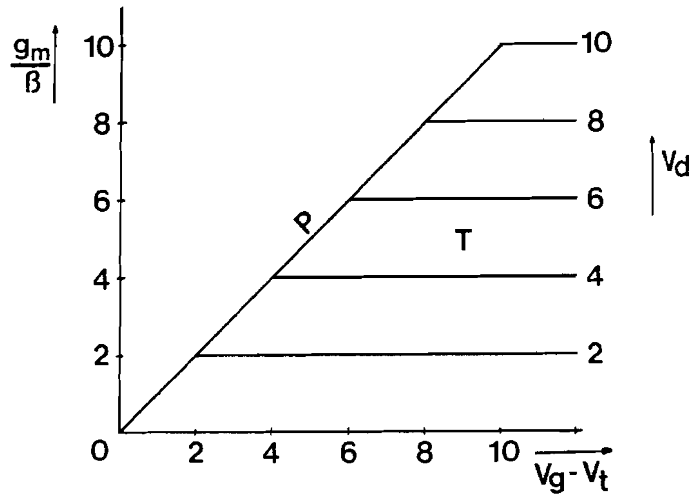

Fig. 3.13. Transconductance vs gate voltage with the drain voltage as parameter. The triode and pentode region are indicated by T and P respectively.

Consider the MOST in a voltage amplifier circuit (see fig. 3.14.).

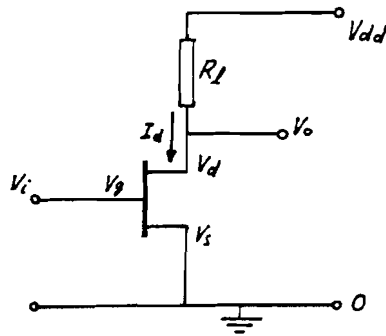

Fig. 3.14. Amplification circuit with a MOST.

The voltage amplification is given by

$$A_v = \frac{V_d}{V_g} = -g_m R_l$$

For a good linearity g_m should be a constant, but as can be seen from Eq. [3.25] and Eq. [3.26] it is proportional to V_d in the triode region and proportional to V_g in the pentode region. This results in non-linearities.

The equations of interest for a two term approximation are joined in Eq. [3.27].

$$\left.\begin{aligned} I_d &= \beta\left[(V_g-V_t)V_d - \frac{V_d^2}{2}\right] \\ I_{d_{sat}} &= \beta\,\frac{(V_g-V_t)^2}{2} \\ g_m &= \beta\, V_d \\ g_{msat} &= \beta\,(V_g-V_t) \\ V_{dsat} &= V_g - V_t \end{aligned}\right\} \qquad [3.27.]$$

If the more accurate three term approximation is considered the equations are given by:

$$\left.\begin{aligned} I_d &= \beta\left[(V_g-V_t)V_d - (1+\delta)\frac{V_d^2}{2}\right] & I_{dsat} &= \beta\,\frac{(V_g-V_t)^2}{2(1+\delta)} \\ g_m &= \beta\, V_d & g_{msat} &= \beta\,\frac{V_g-V_t}{1+\delta} \\ V_{dsat} &= \frac{V_g-V_t}{1+\delta} \end{aligned}\right\} \qquad [3.28.]$$

3.5. <u>Velocity saturation of electrons in silicon</u>

Under nonequilibrium conditions it can be seen (see e.g. fig. 3.10) that the electron density in the channel decreases towards the drain. The current throughout the channel is constant thus the velocity of the electrons must increase towards the drain. The continuity equation for the current is given by

$$I_d = W\,\upsilon(y)\,q\,n(y) = W\,\upsilon(y)\,|Q_n(y)| \qquad [3.29.]$$

where $\upsilon(y)$ is the velocity of the electrons and n(y) is the electron density per unit area.
Furthermore the electron velocity is linearly related to the longitudinal electric field E_y

$$\upsilon(y) = \mu_n E_y(y) = \mu_n \frac{dV(y)}{dy} \qquad [3.30.]$$

With Eq. [3.22], which can be written as

$$\frac{|Q_n(y)|}{C_{ox}} = V_g - V_t - V(y)$$

the differential equation for the potential distribution

V(y) is given by (see appendix C1)

$$-\left[V_g - V_t - V(y)\right] \frac{dV(y)}{dy} = \frac{I_d}{\beta L} \qquad [3.31]$$

The solution with the boundary condition V(0)=0 is

$$V(y) = V_g - V_t - \sqrt{(V_g - V_t)^2 - \frac{2 I_d}{\beta} \frac{y}{L}} \qquad [3.32]$$

The shape of the potential curve V(y) is parabolic.
Substitution of Eq. [3.24] into Eq. [3.32] yields

$$V(y) = (V_g - V_t)\left[1 - \sqrt{1 - \frac{y}{L}}\right] \qquad [3.33]$$

This is the potential distribution if the MOST is pinched off (see fig. 3.10).
As can be seen in fig. 3.9,3.10 the potential gradient increases towards the drain. The potential gradient reaches near-infinity at the pinch off point, thus the electron velocity is considered to be infinite in our model.
When the fields are sufficiently large, however, nonlinearities in mobility and saturation of drift velocity is observed [1 pp. 56-60, 5]. Fig. 3.15 shows the electron velocity as a function of the electric field for silicon.

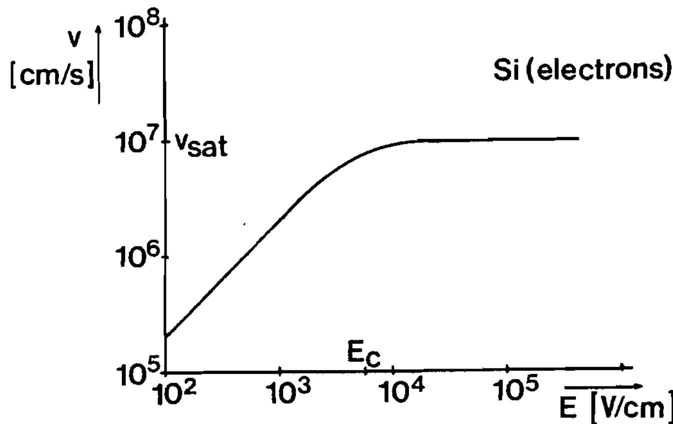

Fig. 3.15. Electron velocity vs electric field for silicon.

The velocity as a function of E_y can be approximated by [3, pp. 550-53]

$$v = \frac{\mu_0}{1 + E_y/E_c} E_y \qquad [3.34]$$

$$\mu_n = \frac{\mu_0}{1 + E_y/E_c} \qquad [3.35]$$

with μ_0 the low field mobility.
For large electric fields Eq. [3.34.] results in

$$v = v_{sat} = \mu_0 E_c \qquad [3.36.]$$

And the potential distribution is given by (see appendix C2)

$$V(y) = V_g - V_t - \frac{I_d}{\beta'} - \sqrt{\left(V_g - V_t - \frac{I_d}{\beta'}\right)^2 - 2\frac{I_d}{\beta'}E_c y} \qquad [3.37.]$$

$$\beta' = W\mu_0 E_c C_{ox} = W v_{sat} C_{ox} \qquad [3.38.]$$

The shape of this potential curve is also parabolic.
At pinch off the minimum channel charge at y=L is given by

$$Q_n(L) = \frac{I_{dsat}}{W\, v_{sat}}$$

$$\frac{Q_n(L)}{C_{ox}} = \frac{I_{dsat}}{\beta'} = V_g - V_t - V_{dsat} \qquad [3.39]$$

This minimum channel charge is linear related to the saturation drain current. As in the previous case $Q_n(L)=0$ gives the pinch off potential at the drain, now Eq [3.39] has to be used (see fig. 3.16).

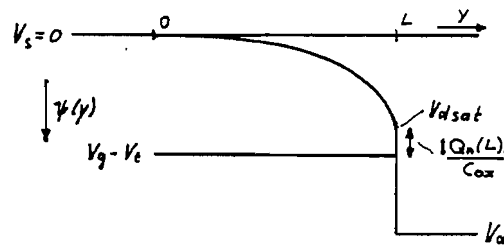

Fig. 3.16. Longitudinal potential distribution of a MOST which operates in the pentode region. Due to the velocity saturation of the electrons, the channel charge does nog equal zero at the pinch off point.

Because the drain current reaches its maximum value at the saturation drain voltage, V_{dsat} can be found by differentiating the drain current equation $\left(\frac{\partial I_d}{\partial V_d} = 0\right)$.

3.6. Device characteristics, adjusted for velocity saturation effects

Due to the electron velocity saturation effects the device characteristics are influenced. This can be seen by considering fig. 3.17 which shows the potential distribution of a MOST in the saturation region, where two different gate voltages are applied ($V_{g2}>V_{g1}$).

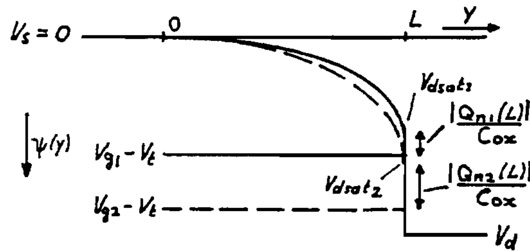

Fig. 3.17. Comparison of the longitudinal potential distribution for two different values of the gate voltage, with $V_{g2} > V_{g1}$, for a MOST which operates in the pentode region. Velocity saturation effects are taken into account.

The channel charge at y=0 and y=L is respectively

$$Q_n(o) = \frac{V_g - V_t}{C_{ox}} \qquad \text{and} \qquad Q_n(L) = \frac{V_g - V_t - V_{dsat}}{C_{ox}}$$

$$\frac{V_{dsat}}{C_{ox}} = \frac{V_g - V_t}{C_{ox}} - Q_n(L) \qquad *$$

Since the drain current increases at increasing V_g-V_t, subsequently $Q_n(L)$ must increase ($Q_n(L)\, v_{sat} W = I_d$).
So, according to (*) V_{dsat} will increase less then proportional to V_g-V_t. As known, the drain current is proportional to V_{dsat}^2, due to the parabolic potential distribution. Because V_{dsat} increases no longer proportional to V_g-V_t, the drain current will no longer increase proportional to $(V_g-V_t)^2$. So linearisation can be expected. This will tend to a horizontal transconductance curve for the pentode region.

The drain current can be found by substitution of Eq. [3.35.] into Eq. [3.11] and solving this equation in a similar way as shown in Appendix A.

$$I_d = \frac{W\mu_0 E_c C_{ox}}{E_c L + V_d}\left\{(V_g - 2\psi_B - \frac{V_d}{2})V_d - \frac{2}{3}\frac{\sqrt{2\varepsilon_s q N_A}}{C_{ox}}\left[(V_d + 2\psi_B - V_b)^{3/2} - (2\psi_B - V_b)^{3/2}\right]\right\} \quad [3.40.]$$

If only two terms of the Taylor expansion are used the following equations will be obtained

$$I_d = \beta' \frac{(V_g - V_t)V_d - \frac{V_d^2}{2}}{E_c L + V_d}$$

$$I_{dsat} = \beta'(V_g - V_t - V_{dsat}) = \beta \frac{V_{dsat}^2}{2E_c L}$$

$$= \beta' E_c L\left\{1 + \frac{V_g - V_t}{E_c L} - \sqrt{1 + 2\frac{V_g - V_t}{E_c L}}\right\}$$

$$g_m = \beta' \frac{V_d}{E_c L + V_d} \quad [3.41.]$$

$$g_{msat} = \beta'\left\{1 - \left(1 + 2\frac{V_g - V_t}{E_c L}\right)^{-1/2}\right\}$$

$$V_{dsat} = E_c L\left\{-1 + \sqrt{1 + 2\frac{V_g - V_t}{E_c L}}\right\}$$

The first equality for I_{dsat} is already given by Eq.[3.39] V_{dsat} follows from $\frac{\partial I_d}{\partial V_d} = 0$. Fig. 3.18 shows the drain current as a function of the drainvoltage with the gate voltage as parameter, for a MOST with a channel length of 4 μm. This will be noted by "4 μ MOST".
The transconductance versus the gate voltage with the drain voltage as parameter is shown in fig. 3.19.

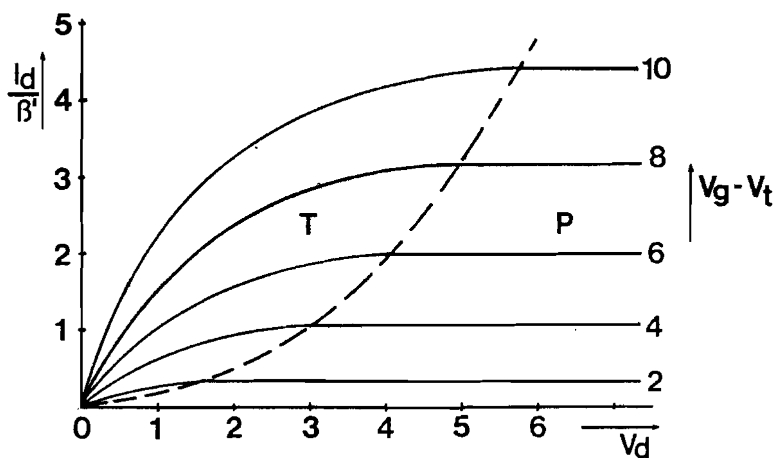

Fig. 3.18. Drain current vs drain voltage with the gate voltage as parameter for a 4 μ MOST. Velocity saturation effects are taken into account, E_c=10.000 V/cm.

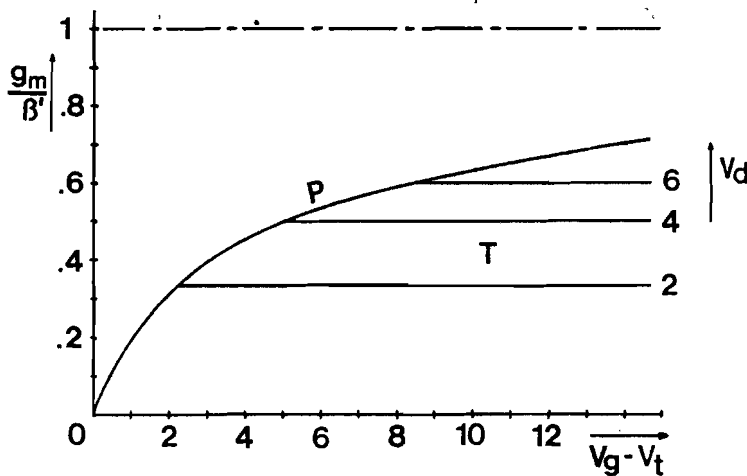

Fig. 3.19. Transconductance vs gate voltage with the drain voltage as parameter for a 4 μ MOST. Velocity saturation effects are taken into account, E_c=10.000 V/cm.

The behaviour of the MOST in the pentode region for large V_g is much more linear. The transconductance has an asymptotic value $\beta' = W v_{sat} C_{ox}$, which is limited, at a given device geometry, by the saturation velocity.
It is observed that this value is independent of the length L of the device.
Fig. 3.20 shows the saturation transductance for three different channellengths. In the short structures the high electric fields are obtained at relatively small applied voltages.

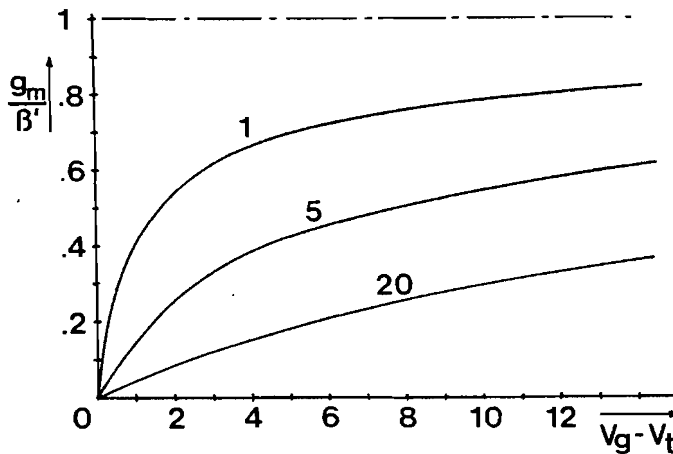

Fig. 3.20. Comparison of the transconductance of three MOSTs in saturation with channellengths of 1 μm, 5 μm and 10 μm. E_c = 10.000 V/cm.

It is desirable to have a linear region for small values of V_g, which can be obtained by shortening the device. This also results in a larger transconductance at the same gate voltage.

If three terms of the Taylor expansion are taken into account the describing equations are

$$\left.\begin{aligned}
I_d &= \beta' \frac{(V_g - V_t)V_d - (1+\delta)\frac{V_d^2}{2}}{E_c L + V_d} \\
I_{dsat} &= \beta' \left(V_g + \Delta V_t - (1+\delta) V_{dsat} \right) = \beta' \frac{V_{dsat}^2}{2(1+\delta) E_c L} \\
&= \beta'(1+\delta) E_c L \left\{ 1 + \frac{V_g - V_t}{(1+\delta) E_c L} - \sqrt{1 + 2\frac{V_g - V_t}{(1+\delta) E_c L}} \right\} \\
g_m &= \beta' \frac{V_d}{E_c L + V_d} \\
g_{msat} &= \beta' \left\{ 1 - \left(1 + 2\frac{V_g - V_t}{(1+\delta) E_c L} \right)^{-1/2} \right\} \\
V_{dsat} &= E_c L \left\{ -1 + \sqrt{1 + 2\frac{V_g - V_t}{(1+\delta) E_c L}} \right\}
\end{aligned}\right\} \quad 3.42 .$$

4. The DMOST

4.1. Introduction

The behaviour of a MOST can be linearized by shortening the channellength. The minimum length is limited by the photo-lithographic process. To overcome this problem a boron diffusion through the source contact hole is proposed.
Due to the large diffusion coefficient of boron, a high doped P-region is formed around the source and two different channel regions are formed under the gate.
By varying the diffusion depth, the length of the first region can be changed.
This kind of structure is called a double-diffused MOST (DMOST).

4.2. Operation modes of the DMOST

Fig. 4.1. shows a DMOST, which is an ordinary MOST, with an high doped P-region around the source region.

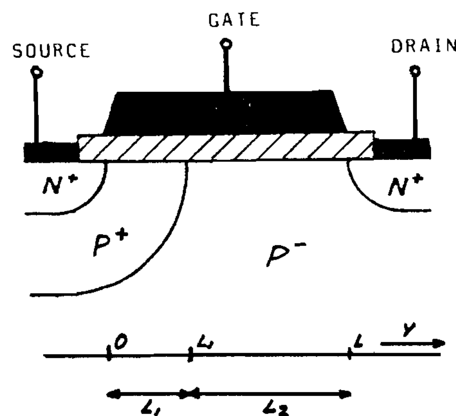

Fig. 4.1. Schematic diagram of a DMOST.

This structure can be considered as two MOSTs connected in series, with a common gate.
The high doped region is called the first channel region and by the second channel region is meant the low doped region.

The difference between the two MOSTs is first the channellength L and second the threshold voltage V_t. This last can be understood from

$$V_t = 2\psi_B + K_P\sqrt{2\psi_B - V_b}$$

and

$$2\psi_B = \frac{2kT}{q}\ln\frac{N_A}{n_i}$$

$$K_P = \frac{\sqrt{2\varepsilon_s q N_A}}{C_{ox}}$$

Due to the higher doping concentration of the first channel region, this MOST has a larger threshold voltage. The first channel of the DMOST is usually shorter than the second one. Under different biasing conditions the individual MOSTs can operate in triode or pentode region. We can distinguish four modes, these are: both MOSTs in triode region, called the TT mode, the first MOST in triode region and the second one in pentode region, called TP mode, or v.v. called the PT mode and last both MOSTs in pentode region, called the PP mode (see fig. 4.2).

1st	2nd	channel
T	T	
T	P	
P	T	
P	P	

Fig. 4.2. The operation modes of a DMOST.

To derive the drain current under given biasing conditions it is necessary to know in which mode the DMOST operates. Then the equations (which are derived in chapter 3) describing the individual MOSTs can be used. Because the potential $V(L_1)$ (see fig. 4.1.) is unknown, which is the

source voltage of the second MOST and the drain voltage of the first one, we do not know the operation mode of the DMOST. To overcome this problem, consider the situation at which both MOSTs just pinch off simultaneously. Fig. 4.3. shows the potential distribution of two MOSTs in series, for that situation. In order to connect the potential curves correctly, the channel potential V(y) and the gate voltage V_g must be continuous at the boundary. At a first glance it seems that this prescribes the difference in threshold voltage. Since this voltage difference is given, this situation can only be realised at one particular gate voltage.

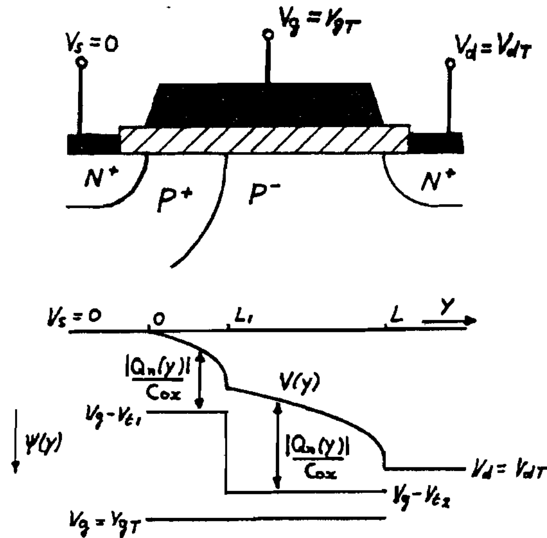

Fig. 4.3. Longitudinal potential distribution of a DMOST where both channels just pinch off simultaneously.

The subscript 1 and 2 will be used for the first and second MOST respectively. The gate voltage and drain voltage in this situation are called V_{gT} and V_{dT}. By increasing V_d ($V_d > V_{dT}$) the channelpotentialV(y) is unchanged because the extra drain voltage appears beyond the second pinch off point. When we decrease V_d ($V_d < V_{dT}$) both MOSTs operate in the triode region.

This can be seen by the following considerations. If the drain voltage is lowered, the current in both MOSTs decreases. The current has its maximum value at saturation. Thus now both MOSTs are in the triode region.

Next consider the situation with $V_g > V_{gT}$ at a large value of V_d (see fig. 4.4)

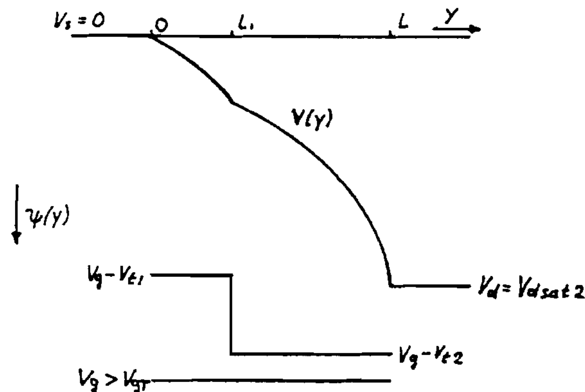

Fig. 4.4. Longitudinal potential distribution of a DMOST for $V_g > V_{gT}$, where the second channel just pinches off.

It will be shown that for sufficient large V_d the first MOST operates in the triode region while the second one operates in the pentode region. The shape of the potential curve $V(y)$ can be explained by the following considerations. For large gate voltages the step in the $V_g - V_t$ curve is relatively small. If one neglects this voltage step, there would be no dip in the potential curve $V(y)$ at all. Due to a small step, the charge in the first channel is only slightly less than in the second one around $y = L_1$. Therefore, around $y = L_1$, the potential gradient can not differ too much and the dip will be small. Owing to this situation the first MOST operates in the triode region, while the second can operate in the pentode region. Increasing V_d ($V_d > V_{dsat2}$) the extra drain voltage appears beyond the pinch off region. If V_d is decreased ($V_d < V_{dsat2}$) eventually both MOSTs operate in the triode region. Thus for $V_g > V_{gT}$ the DMOST operates in the TT mode if $V_d < V_{dsat2}$ and in the TP mode if $V_d > V_{dsat2}$.
Now, consider the situation for $V_g < V_{gT}$ (see fig. 4.5). Starting with $V_d = 0$ and increasing this voltage, we see that both MOSTs operate in the triode region. Due to the relatively large step in the $V_g - V_t$ curve there is considerable less

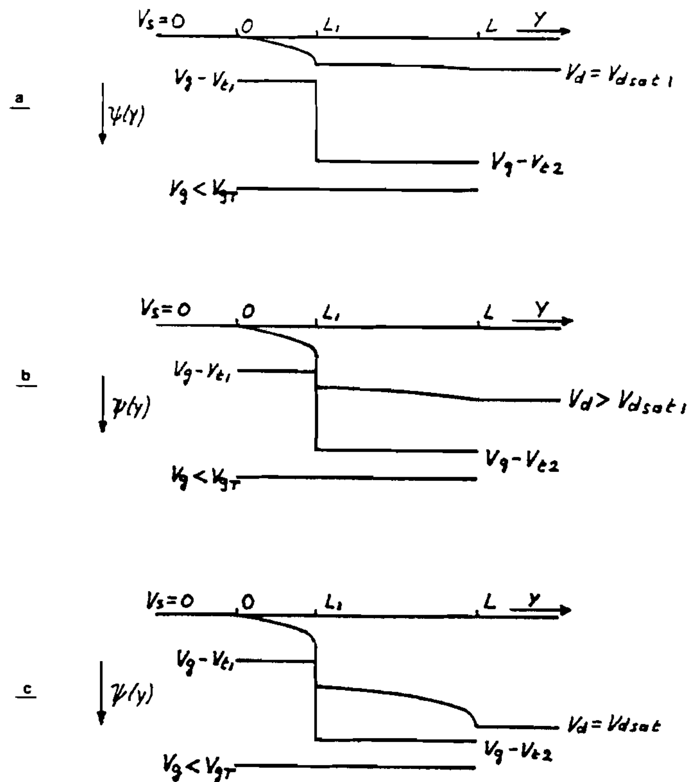

Fig. 4.5. Longitudinal potential distribution of a DMOST for $V_g < V_{gT}$, while
a. the first channel just pinches off.
b. the first channel is pinched off and the second channel still is in triode region,
c. the first channel is pinched off and the second channel just pinches off.

charge in the first channel then in the second one. This results in a large potential gradient in the first channel, and this MOST will pinch off first by increasing the drain potential (fig. 4.5.a). The current of this MOST has reached its maximum value.

By further increase of the drain voltage, the source potential of the second MOST establishes in such a way that the current in this MOST equals the first MOST saturation current, both for triode (see fig. 4.5.b.) and pentode region (see fig. 4.5.c.). In this situation an arbitrary voltage drop can appear beyond the first pinch off point. If the second MOST also saturates the extra drain voltage appears beyond the second pinch off point. Thus, if $V_g<V_{gT}$ the DMOST operate in the TT mode for sufficiently small drain voltage, then in the PT mode for higher drain voltage and finally in the PP mode for $V_d> V_{dsat}$. In fig. 4.6. a review of the different modes is shown.

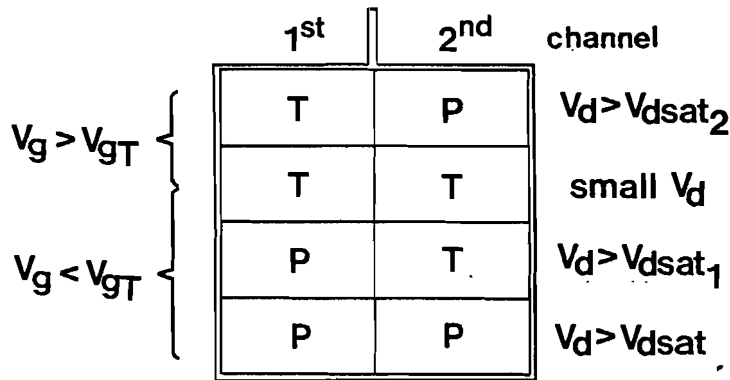

Fig. 4.6. Review of the operation modes of the DMOST under different biasing conditions.

4.3. The transition mode of the DMOST

To derive the basic device characteristics, the equation set Eq. [3.41] will be used, at which velocity saturation effects are involved. The drain current equations for the first MOST are given by

$$I_d = \beta' \frac{V_g' V_c - V_c^2/2}{E_c L_1 + V_c} \qquad [4.1]$$

$$\begin{aligned} I_{dsat} &= \beta'(V_g' - V_{csat}) \\ &= \beta' E_c L_1 \left\{ 1 + \frac{V_g'}{E_c L_1} - \sqrt{1 + 2\frac{V_g'}{E_c L_1}} \right\} \end{aligned} \qquad [4.2]$$

with $V_g' = V_g - V_{t1}$

V_c is the common voltage for the drain of the first channel and for the source of the second one. The drain current equations for the second MOST are given by

$$I_d = \beta' \frac{(V_g' + \Delta V_t - V_c)(V_d - V_c) - (V_d - V_c)^2/2}{E_c L_2 + (V_d - V_c)} \qquad [4.3.a]$$

$$= \beta' \frac{(V_g' + \Delta V_t)(V_d - V_c) - \frac{V_d^2 - V_c^2}{2}}{E_c L_2 + (V_d - V_c)} \qquad [4.3.b]$$

$$\begin{aligned} I_{dsat} &= \beta'\left((V_g' + \Delta V_t - V_c) - (V_{dsat} - V_c)\right) = \beta'(V_g' + \Delta V_t - V_c) \\ &= \beta' E_c L_2 \left\{ 1 + \frac{V_g' + \Delta V_t - V_c}{E_c L_2} - \sqrt{1 + 2\frac{V_g' + \Delta V_t - V_c}{E_c L_2}} \right\} \end{aligned} \qquad [4.4]$$

with $\Delta V_t = V_{t1} - V_{t2} > 0$ thus $V_g' + \Delta V_t = V_g - V_{t2}$

It should be noticed that β' for both channels is equal. It is obvious that a channel from source to drain is formed only if V_g exceeds the threshold voltage of the first MOST, so V_{t1} is the over-all threshold voltage. This condition corresponds with $V_g' > 0$.
It is shown in the previous subsection that we can deduce the operation mode in any biasing condition without knowing V_c explicitely. The main parameter in this consideration is V_{gT}, the transition gate voltage [4] . V_{gT} is defined as the gate voltage at which both MOSTs just pinch off simultaneously. The common voltage is given by the saturation drain voltage of the first MOST; and is called V_{cT} in this situation (see Eq. [3.41.]).

$$V_{cT} = E_c L_1 \left\{ -1 + \sqrt{1 + 2\frac{V_{gT}'}{E_c L_1}} \right\} \qquad [4.5.]$$

The saturation drain current in the first and second MOST is respectively

$$I_{dsatT} = \beta'(V_{gT}' - V_{cT}) \qquad [4.6.]$$

$$I_{dsatT} = \beta' \left\{ E_c L_2 + V_{gT}' + \Delta V_t - V_{cT} - E_c L_2 \sqrt{1 + 2\frac{V_{gT}' + \Delta V_t - V_{cT}}{E_c L_2}} \right\} \qquad [4.7.]$$

Equating the last two formulas and substitution of Eq. [4.5] into the square root term of Eq. [4.7.] yields

$$V_{gT}' = \frac{(\Delta V_t)^2}{2 E_c L_2} + \Delta V_t \sqrt{\frac{E_c L_1}{E_c L_2}} \qquad [4.8.]$$

Substitution of Eq. [4.8.] into Eq. [4.5] yields

$$V_{cT} = \Delta V_t \sqrt{\frac{E_c L_1}{E_c L_2}} \qquad [4.9.]$$

and substitution of Eq. [4.8] and Eq. [4.9] into Eq. [4.6] yields

$$I_{dsatT} = \beta' \frac{\Delta V_t^2}{2 E_c L_2} \qquad [4.10]$$

For the second MOST the saturation drain current can also be written as

$$I_{dsatT} = \beta'\left((V_{gT}' + \Delta V_t - V_{cT}) - (V_{dT} - V_{cT})\right) \qquad [4.11.]$$

Substitution of Eq. [4.6.] into this equation yields

$$V_{dT} - V_{cT} = \Delta V_t \qquad [4.12]$$

This is not amazing, because through both pinch off regions the same current flows. The difference in effective gate voltage ($V_g - V_t$) is ΔV_t, so the difference in channel potential must also be ΔV_t. (see fig. 4.7).

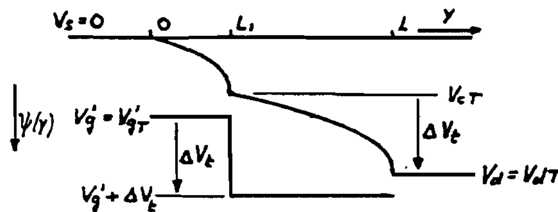

Fig. 4.7. Longitudinal potential distribution at $V_g=V_{gT}$. It is seen that $Qn(L_1)=Qn(L)$ is this situation.

Example

First region $V_{t1} = 5V$ Second region $V_{t2} = 1V$

$L_1 = 1\ \mu m$ $L_2 = 4\mu m$

$E_c = 10.000\ V/cm$, so $E_c L_1 = 1V$

$E_c L_2 = 4V$

$\Delta V_t = 4V$

The transition gate voltage follows from Eq. [4.8]

$$V'_{gT} = \frac{(\Delta V_t)^2}{2 E_c L_2} + \Delta V_t \sqrt{\frac{E_c L_1}{E_c L_2}} = 4\ V$$

With $V'_g = V_g - V_{t1}$ it follows that $V_{gT} = 9V$.
The common voltage at the transition situation is (Eq. [4.5])

$$V_{cT} = E_c L_1 \left[-1 + \sqrt{1 + 2\frac{V'_{gT}}{E_c L_1}}\right]$$

$$= 1 \quad \left[-1 + \sqrt{1 + 2\ \frac{4}{1}}\right] = 2\ V$$

and the drain voltage V_{dT} is given by Eq. [4.12.]

$$V_{dT} = V_{cT} + \Delta V_t = 6\ V$$

Finally the draincurrent in this situation can be found with Eq. [4.6.] or Eq. [4.10].

$$\frac{I_{dsatT}}{\beta'} = V_{gT}' - V_{cT} = \frac{(\Delta V_t)^2}{2 E_c L_2} = 2\ V$$

These results are shown in fig. 4.11.

4.4. Basic device characteristics

For $V_g < V_{gT}$ and increasing V_d from zero, a situation will be reached at which the first MOST starts to saturate. (see fig. 4.5 a).

The drain voltage at which this happens will be called V_{dsat1}. The current in this situation is determined by the first MOST

$$I_{dsat} = \beta'(V_g' - V_{csat}) \qquad [4.13.]$$

with $$V_{csat} = E_c L_1 \left\{ -1 + \sqrt{1 + \frac{2 V_g'}{E_c L_1}} \right\} \qquad [4.14.]$$

The second MOST operates in the triode region and its current is prescribed by Eq. [4.13]. Substitution of this equation into Eq. [4.3 a] with $V_c = V_{csat}$ yields the potential difference across the second channel.

$$V_{dsat1} - V_{csat} = \Delta V_t - \sqrt{(\Delta V_t)^2 - 2 E_c L_2 (V_g' - V_{csat})} \qquad [4.15.]$$

(By solving the quadratic equation only the - sign holds because now the potential across the second channel is less than the potential across the second channel in the transition situation).

If $V_d < V_{dsat1}$, the DMOST operates in the TT mode and for $V_d > V_{dsat1}$ the DMOST operates in the PT or PP mode. In this last situation the draincurrent is completely determined by the first channel and to this situation is also referred as the first channel control region [4] . The draincurrent in these modes is given by

$$I_{dPT} = I_{dPP} = \beta' E_c L_1 \left\{ 1 + \frac{V_g'}{E_c L_1} - \sqrt{1 + 2\frac{V_g'}{E_c L_1}} \right\} \qquad [4.16.]$$

Just as in the transition situation the drainvoltage at which the second channel saturates is given by (see fig. 4.8.)

$$V_{dsat} = V_{csat} + \Delta V_t$$

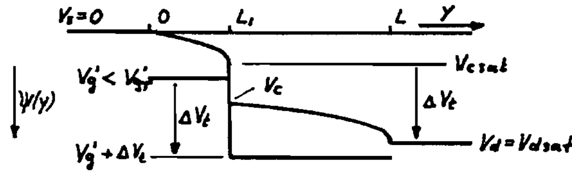

Fig. 4.8. Longitudinal potential distribution for $V_g > V_{gT}$ if the DMOST operates in the PP-mode. It is seen that Qn(L1) = Qn(L) in this situation.

If a gate voltage above the transition gate voltage is applied ($V_g > V_{gT}$) the second channel pinches only at sufficient large drain voltage. To evaluate this saturation drain voltage (V_{dsat2}) the common voltage, called V_{c2} in this situation, must be calculated first.
This can be done by equating the current equations Eq. [4.1] for the first MOST and Eq. [4.4] for the second MOST. (see Appendix D1).

$$V_{c2} = E_c L_2 + \Delta V_t - \sqrt{(E_c L_2 + \Delta V_t)^2 + 2 E_c L_2 (V_g' - V_{gT}')} - E_c L_1 + \sqrt{\left[E_c L_2 + \Delta V_t - \sqrt{(E_c L_2 + \Delta V_t)^2 + 2 E_c L_2 (V_g' - V_{gT}')}\right]^2 + \left[E_c L_1 + V_g'\right]^2 - \left[V_g'\right]^2} \qquad [4.17.]$$

And V_{dsat2} is given by

$$V_{dsat2} = V_{c2} + E_c L_2 \left\{ -1 + \sqrt{1 + 2\frac{V_g' + \Delta V_t - V_{c2}}{E_c L_2}} \right\} \qquad [4.18.]$$

It should be noted, that there is a very little error in Eq. [4.17.] which approaches zero if $V_g' \rightarrow V_{gT}'$. (see Appendix D1).
For $V_d < V_{dsat2}$ the DMOST operates in the TT mode and for $V_d > V_{dsat2}$ the DMOST operates in the TP mode.
This last mode is also called the second channel control region, however, the current is determined by the whole structure.
The drain current in this mode follows from Eq. [4.4.]

$$I_{dTP} = \beta' (V_g' + \Delta V_t - V_{dsat2}) \qquad [4.19.]$$

If the drainvoltage is sufficiently small, i.e. $V_d < V_{dsat1}$ for $V'_g < V'_{gT}$ and $V_d < V_{dsat2}$ for $V'_g > V'_{gT}$, the DMOST operates in the

TT mode. The drain current is determined by both MOSTs and can be derived if V_c is known. V_c can be found most easily by rewriting Eq. [4.1.] and Eq. [4.3.b.] and taking the sum, which yields

$$I_d = \beta' \frac{-\Delta V_t V_c + (V_g + \Delta V_t) V_d - \frac{V_d^2}{2}}{E_c L + V_d} \qquad [4.20.]$$

with $L = L_1 + L_2$.

Since this current also is given by Eq. [4.1.] , V_c can be solved. The result is

$$V_c = E_c L_1 \frac{V_g + \Delta V_t - V_d^2/2}{V_g E_c L + \Delta V_t (E_c L_1 - V_d) + V_d^2/2} \quad \text{for } V_d = 2\Delta V_t - E_c L$$

$$V_c = \frac{V_g' E_c L + \Delta V_t (E_c L_1 - V_d) + V_d^2/2}{E_c L + V_d - 2\Delta V_t}$$

$$[4.21.]$$

$$\pm \sqrt{\left[\frac{V_g' E_c L + \Delta V_t (E_c L_1 - V_d) + V_d^2/2}{E_c L + V_d - 2\Delta V_t}\right]^2 - E_c L_1 V_d \frac{2(V_g' + \Delta V_t) - V_d}{E_c L + V_d - 2\Delta V_t}}$$

+ sign if $V_d < 2\Delta V_t - E_c L$

− sign if $V_d > 2\Delta V_t - E_c L$

It is seen by numerical calculations that the + sign must be used if $V_d < 2\Delta V_t - E_c L$ and the − sign only holds if $V_d > 2\Delta V_t - E_c L$. Finally the drain current can be found by substituting Eq. [4.21] into Eq. [4.20] . In the TT mode the drain current as well as the transconductance depends on the drain voltage, so we are less interested in this mode.

Table 4.9. shows a review of the drain current and transconductance in the different modes, as well as the boundaries of the modes. The derivation of g_{mTP} is given in Appendix D2.

$V_g' < V_{gT}$	$V_{gT} = \frac{[illegible]}{2E_cL_2} + \Delta V_t \sqrt{\frac{[illegible]}{E_cL_2}}$ $\qquad V_g > V_{gT}$
$V_{dsat1} = V_{csat} + \Delta V_t - \sqrt{(\Delta V_t)^2 - 2E_cL_2(V_g' - V_{csat})}$ $V_{csat} = E_cL_1\left[-1 + \sqrt{1 + \frac{2V_g'}{E_cL_1}}\right]$	$V_{dsat2} = V_{c2} + E_cL_2\left[-1 + \sqrt{1 + 2\frac{V_g' + \Delta V_t - V_{c2}}{E_cL_2}}\right]$ $V_{c2} = E_cL_2 + \Delta V_t - \sqrt{(E_cL_2 + \Delta V_t)^2 + 2E_cL_2(V_g' - V_{gT}')} - E_cL_1 + \sqrt{\left[E_cL_2 + \Delta V_t - \sqrt{(E_cL_2 + \Delta V_t)^2 + 2E_cL_2(V_g' - V_{gT}')}\right]^2 + \left[E_cL_1 + V_g'\right]^2 - \left[V_g'\right]^2}$
$V_d > V_{dsat1}$ **PT/PP** $I_{dPT} = I_{dPP} = \beta'(V_g' - V_{csat})$ $g_{mPT} = g_{mPP} = \beta'\left[1 - \left(1 + 2\frac{V_g'}{E_cL_1}\right)^{-1/2}\right]$	$V_d > V_{dsat2}$ **TP** $I_{dTP} = \beta'(V_g' + \Delta V_t - V_{dsat2})$ $g_{mTP} = \beta'\left(1 - \frac{dV_{c2}}{dV_g'}\right)\left[1 - \left(1 + 2\frac{V_g' + \Delta V_t - V_{c2}}{E_cL_2}\right)^{-1/2}\right]$ $\frac{dV_{c2}}{dV_g'} = \frac{(E_cL_1 + V_{c2})\left(1 + 2\frac{V_g' + \Delta V_t - V_{c2}}{E_cL_2}\right)^{-1/2} - E_cL_1}{(E_cL_1 + V_{c2})\left(1 + 2\frac{V_g' + \Delta V_t - V_{c2}}{E_cL_2}\right)^{-1/2} - E_cL_1 + E_cL_2 + \Delta V_t - V_{c2} - E_cL_2\sqrt{1 + 2\frac{V_g' + \Delta V_t - V_{c2}}{E_cL_2}}}$
$V_d < V_{dsat1}$ or $V_d < V_{dsat2}$ $I_{dTT} = \beta'\frac{-\Delta V_t V_c + (V_g' + \Delta V_t)V_d - V_d^2/2}{E_cL + V_d}$ $g_{mTT} = \beta'\frac{-\Delta V_t\, \partial V_c/\partial V_g' + V_d}{E_cL + V_d}$	**TT** $V_c = \frac{V_g' + \Delta V_t - V_d^2/2}{V_g'E_cL + \Delta V_t(E_cL_1 - V_d) + V_d^2/2}$ for $V_d = 2\Delta V_t - E_cL$ $V_c = \frac{V_g'E_cL + \Delta V_t(E_cL_1 - V_d) + V_d^2/2}{E_cL + V_d - 2\Delta V_t} \pm \sqrt{\left[\frac{V_g'E_cL + \Delta V_t(E_cL_1 - V_d + V_d^2/2}{E_cL + V_d - 2\Delta V_t} - E_cL_1V_d\frac{2(V_g' + \Delta V_t) - V_d}{E_cL + V_d - 2\Delta V_t}\right.}$ $+$ for $V_d < 2\Delta V_t - E_cL$ $-$ for $V_d > 2\Delta V_t - E_cL$

Table 4.9. Overall picture of the DMOST current and transconductance formulas, and also the potential boundaries of the different modes.

$V_g' < V_{gT}'$	$V_{gT}' = \frac{1+\delta_1}{E_cL_1}\frac{V_{cT}^2}{2} + (1+\delta_1)V_{cT} = \frac{(\Delta V_t + \delta_1 V_{cT})^2}{2(1+\delta_2)E_cL_2} + (1+\delta_1)V_{cT}$ $\qquad V_{cT} = \frac{\Delta V_t\delta_1}{(1+\delta_1)(1+\delta_2)L_1/L_2 - \delta_1^2}\left[1 + \sqrt{\frac{(1+\delta_1)(1+\delta_2)}{\delta_1^2}\frac{E_cL_1}{E_cL_2}}\right]$ $\qquad V_g' > V_{gT}'$
$V_{dsat1} = \frac{(1+\delta_1+\delta_2)V_{csat} + \Delta V_t}{1+\delta_2} - \sqrt{\left(\frac{\delta_1 V_{csat} + \Delta V_t}{1+\delta_2}\right)^2 - 2\frac{E_cL_2}{1+\delta_2}(V_g' - (1+\delta_1)V_{csat})}$ $V_{csat} = E_cL_1\left[-1 + \sqrt{1 + \frac{2V_g'}{(1+\delta_1)E_cL_1}}\right]$	$V_{dsat2} = V_{c2} + E_cL_2\left[-1 + \sqrt{1 + 2\frac{V_g' + \Delta V_t - V_{c2}}{(1+\delta_2)E_cL_2}}\right]$ $V_{c2} = \frac{b}{1-\delta_1} + \sqrt{\frac{b^2}{(1-\delta_1)^2} + \frac{c}{1-\delta_1}}$ for $0 \le \delta_1 < 1$ $V_{c2} = -c/2b$ for $\delta_1 = 1$ $V_{c2} = \frac{b}{1-\delta_1} - \sqrt{\frac{b^2}{(1-\delta_1)^2} + \frac{c}{1-\delta_1}}$ for $\delta_1 > 1$ with: $b = (1+\delta_2)E_cL_2\left[1 - \sqrt{1 + 2\frac{V_g' + \Delta V_t - V_{cT}}{(1+\delta_2)E_cL_2}}\right] - E_cL_1 + \Delta V_t$ $c = 2E_cL_1\left[b + E_cL_1 + V_g'\right]$
$V_d > V_{dsat1}$ **PT/PP** $I_{dPT} = I_{dPP} = \beta'(V_g' - (1+\delta_1)V_{csat})$ $g_{mPT} = g_{mPP} = \beta'\left[1 - \left(1 + 2\frac{V_g'}{(1+\delta_1)E_cL_1}\right)^{-1/2}\right]$	$V_d > V_{dsat2}$ **TP** $I_{dTP} = \beta'(V_g' + \Delta V_t - (1+\delta_2)V_{dsat2} + \delta_2 V_{c2})$ $g_{mTP} = \beta'\left(1 - \frac{dV_{c2}}{dV_g'}\right)\left[1 - \left(1 + 2\frac{V_g' + \Delta V_t - V_{c2}}{(1+\delta_2)E_cL_2}\right)^{-1/2}\right]$ $\frac{dV_{c2}}{dV_g'} = \frac{(E_cL_1 + V_{c2})\left(1 + 2\frac{V_g' + \Delta V_t - V_{c2}}{(1+\delta_2)E_cL_2}\right)^{-1/2} - E_cL_1}{(E_cL_1 + V_{c2})\left(1 + 2\frac{V_g' + \Delta V_t - V_{c2}}{(1+\delta_2)E_cL_2}\right)^{-1/2} - E_cL_1 + (1+\delta_2)E_cL_2 + \Delta V_t - (1-\delta_1)V_{c2} - (1+\delta_2)E_cL_2\sqrt{1 + 2\frac{V_g' + \Delta V_t - V_{c2}}{(1+\delta_2)E_cL_2}}}$
$V_d < V_{dsat1}$ or $V_d < V_{dsat2}$ $I_{dTT} = \beta'\frac{-(\Delta V_t - \delta_2 V_d)V_c + (V_g' + \Delta V_t)V_d - \frac{V_d^2}{2}(1+\delta_2) - \frac{V_c^2}{2}(\delta_1+\delta_2)}{E_cL + V_d}$ $g_{mTT} = \beta'\frac{-(\Delta V_t - \delta_2 V_d)\, dV_c/dV_g' + V_d - V_c\, dV_c/dV_g'\,(\delta_1+\delta_2)}{E_cL + V_d}$	**TT** $V_c = a_0/2a_1$ for $a_2 = a_3V_{cT}$ $V_c = \frac{a_1}{a_2 - a_3V_{cT}} \pm \sqrt{\left(\frac{a_1}{a_2 - a_3V_{cT}}\right)^2 - \frac{a_0}{a_2 - a_3V_{cT}}}$ $\quad$ $+$ for $a_2 < a_3V_{cT}$, $-$ for $a_2 > a_3V_{cT}$ $\frac{dV_c}{dV_g'} = \frac{2E_cLV_c - 2E_cL_1V_d}{-3a_3V_c^2 + 2a_2V_c - 2a_1}$ with: $a_3 = \delta_1 + \delta_2$ $a_2 = (1+\delta_1)E_cL + (1+\delta_1+2\delta_2)V_d - 2\Delta V_t - (\delta_1+\delta_2)E_cL_1$ $a_1 = \Delta V_t(E_cL_1 - V_d) - \delta_2E_cL_1V_d + E_cLV_g' + (1+\delta_2)V_d^2/2$ $a_0 = 2E_cL_1V_d\left[V_g' + \Delta V_t - V_d/2\,(1+\delta_2)\right]$

Table 4.10. DMOST formulas, derived from the more accurate MOST equation set Eq. [3.41] .

Table 4.10. shows an overall picture of the drain current and transconductance in the different modes if the more accurate equation set Eq. [3.42] is used. At the derivation of V_c in the TT mode a cubic equation appears. This equation can be approximated by setting $(V_c)^3$ to $(V_c)^2 V_{cT}$, which results in a quadratic equation and the error approaches zero around the transition situation.
Fig. 4.11. and 4.12. show the draincurrent vs the drainvoltage with V_g

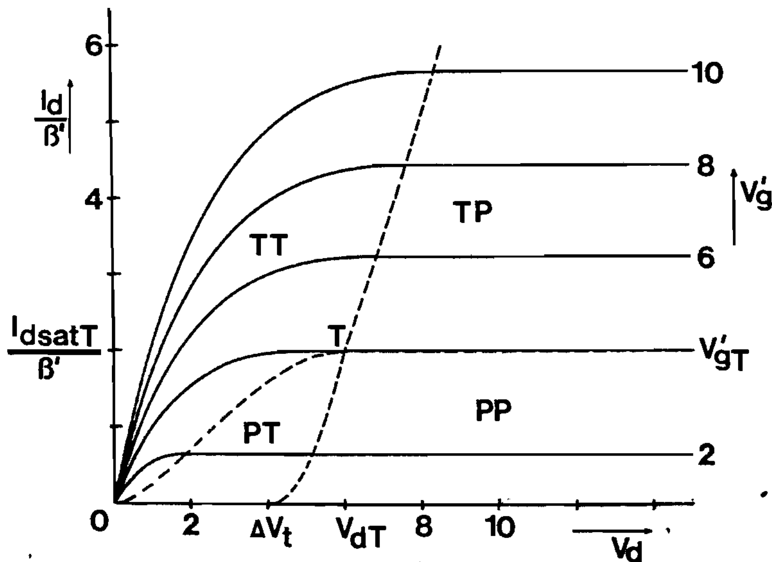

Fig.4.11. Drain current vs drain voltage with the gate voltage as parameter for a 5 μ DMOST with L_1=1 μm, ΔV_t = 4V, and E_c=10.000 V/cm. The dashed curves separates the areas with the different modes. The transition point is indicated by T.

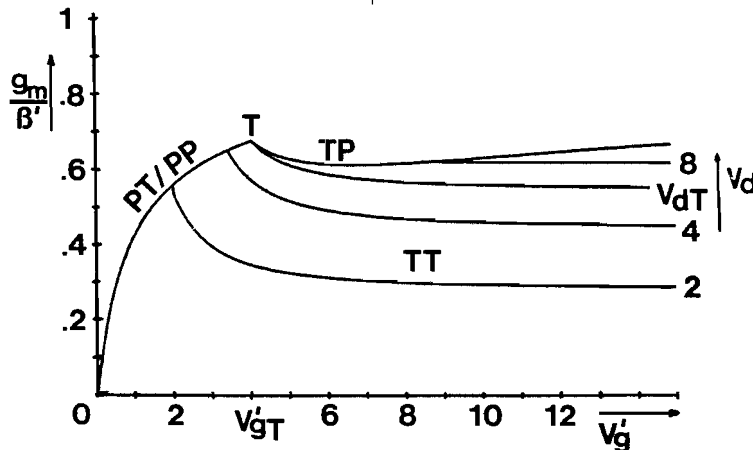

Fig.4.12. Transconductance vs gate voltage with the drain voltage as parameter for a 5 μ DMOSt with L_1= 1 μm, ΔV_t=4 V, E_c=10.000 V/cm. The transition point is indicated by T.

as parameter, and the transconductance versus gate voltage with V_d as parameter respectively. In this last diagram an anomalous behaviour is observed. Considering the situation with the second channel is pinched off, the transconductance increases with increasing V'_g, just as at an ordenary MOST. But if V'_g exceeds V'_{gT} the transconductance first decreases and later on it increases again. This behaviour can be explained by the following considerations.

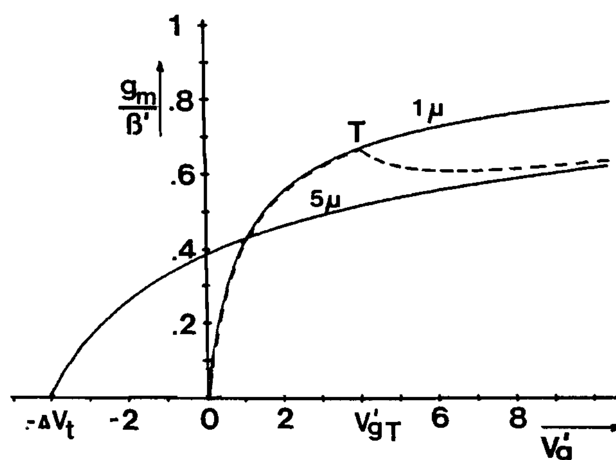

Fig.4.13. Transconductance vs gate voltage for a 1 μ MOST and a 5 μ MOST (shifted ΔV_t to the left) both operating in the pentode region (solid curves) and for a 5 μ DMOST with L_1=1 um ΔV_t = 4 V and E_c=10.000 V/cm, operating in the TP and PP mode (dashed curve).

In fig. 4.13. the transconductance for a 1 μm MOST and a 5 μm MOST is shown, (solid curves) according to a DMOST with a total length of 5 μm and a first channellength of 1 μm (dashed curve). For $V'_g < V'_{gT}$ the transconductance is completely determined by the first channel, which corresponds with an ordinary 1μ MOST while the transductance is determined by a 5 μm structure if $V_g > V_{gT}$. For large V'_g the difference in threshold voltage ΔV_t is relatively small and can be neglected.
Then the behaviour of the DMOST corresponds with a 5 μm MOST with a threshold voltage equal to the threshold voltage of the

second channel. We will refer to this as the "basic" MOST, because this structure is equal to the MOST before the boron diffusion is done. By decreasing the gate voltage the threshold voltage difference becomes more important. The DMOST curve will differ more and more from the basic MOST curve.

If the transconductance of the basic MOST is considerably lower than the transconductance of the first channel MOST at the transition point, the DMOST shows a dip in the transconductance curve. This will be the case if the second channel is much longer than the first one.

For large threshold voltage difference, ΔV_t the basic MOST curve shifts to the left, while the transition gate voltage is increased; so the dip decreases.

Fig. 4.14. shows the transconductance for different second channellengths and different threshold voltage differences.

The change in transition gate voltage can easily be explained by considering the longitudinal voltage distribution and is left to the reader. (see Eq. [4.8.]).

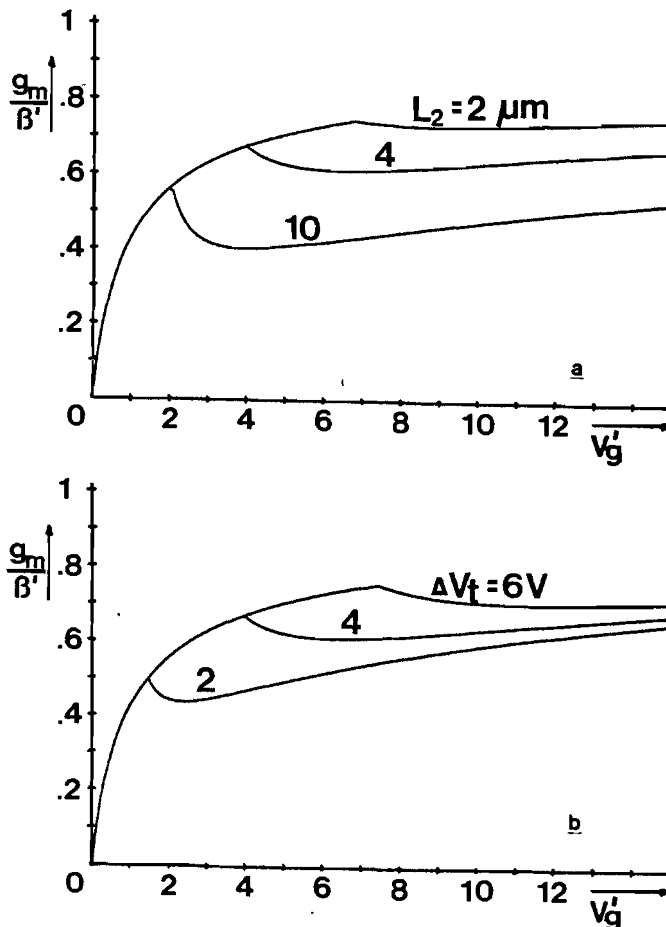

Fig. 4.14. Transconductance dependency of a DMOST with L_1=1 µm, due to
a. second channellength variations, at ΔV_t=4V.
b. variations in the threshold voltage difference, for L=5 µm.

Although, the equations are given in closed form, the calculation of the transconductance in the TP mode is rather laborious. This is caused by the variation in the common voltage. At each biasing condition this voltage and its deravitive must be calculated. (see tables 4.9. and 4.10.). We will make a small error, however, if we assume V_{c2} to be equal to V_{cT}. Although this is now a constant, we can not take

$\frac{\partial V_{c2}}{\partial V_g'} = 0$, because the approximation must be carried out in the final equation (see Appendix D2). The error will be negligible small for $V'_g \approx V'_{gT}$ and for large V'_g, because then the difference between

$V_g' + \Delta V_t - V_{c2}$ and $V_g' + \Delta V_t - V_{cT}$ is relatively small (see figure in Appendix D1).

By this approximation the square root, in the transconductance equation g_{mTP}, is only dependent on V'_g and will be noted as

$$S(V_g') = \sqrt{1 + \frac{V_g' + \Delta V_t - V_{cT}}{E_c L_2}} \qquad [4.22.]$$

Then the transconductance is given by

$$g_{mTP} = \beta'\left(1 - \frac{\partial V_{c2}}{\partial V_g'}\right)\left\{1 - S^{-1}(V_g')\right\} \qquad [4.23.]$$

$$\frac{\partial V_{c2}}{\partial V_g'} = \frac{(E_cL_2 + V_{cT})\,S^{-1}(V_g') - E_cL_1}{(E_cL_2 + V_{cT})\,S^{-1}(V_g') - E_cL_1 + E_cL_2 + \Delta V_t - V_{cT} - E_cL_2\,S(V_g')}$$

where $S(V_g')$ is the only variable.

Fig. 4.15. shows a comparison of the approximated curve (dashed curve) and the exact curve (solid curve).

This approximation is also applicable to the more accurate equation set from table (4.10) and is given by

$$g_{mTP} = \beta'\left(1 - \frac{\partial V_{c2}}{\partial V_g'}\right)\left\{1 - S_\delta^{-1}(V_g')\right\}$$

$$\frac{\partial V_{c2}}{\partial V_g'} = \frac{(E_cL_1 + V_{cT})\cdot S_\delta^{-1}(V_g') - E_cL_1}{(E_cL_1 + V_{cT})\cdot S_\delta^{-1}(V_g') - E_cL_1 + (1+\delta_2)E_cL_2 + \Delta V_t - (1-\delta_1)V_{cT} - (1+\delta_2)E_cL_2\,S_\delta(V_g')}$$

with $S_\delta(V_g') = \sqrt{1 + \frac{V_g' + \Delta V_t - V_{cT}}{(1+\delta_2)\,E_c L_2}}$

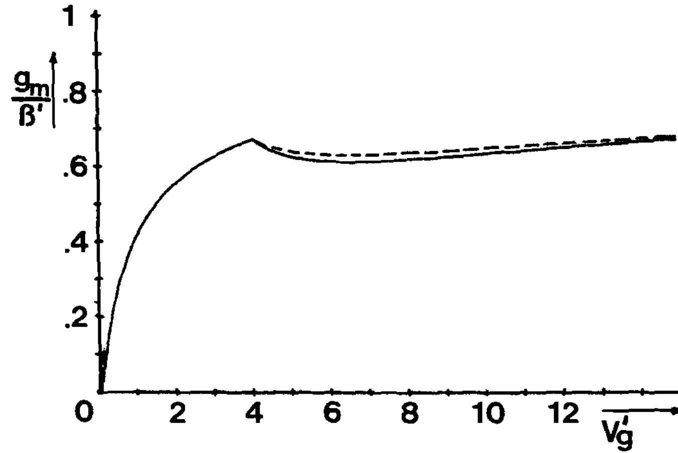

Fig. 4.15. Comparison of the approximated transconductance curve (dashed curve) and the curve obtained by the equation set of Fig. 4.9 (solid curve) for a 5 μ DMOST with L_1=1 um, ΔV_t=4V and E_c=10.000 V/cm.

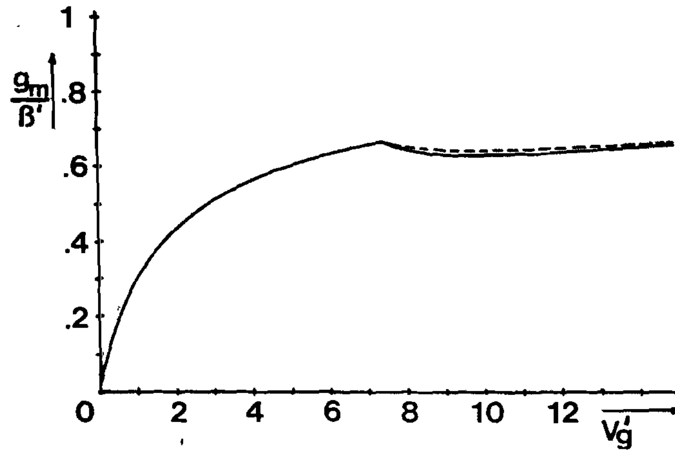

Fig. 4.16. Comparison of the approximated transconductance curve (dashed curve) and the curve obtained by the equation set of Fig. 4.10 (solid curve) for a 5 μ DMOST with L_1= 1 μm, V_t=4 V, δ_1=1, δ_2=0.2 and E_c=10.000 V/cm.

It should be noticed that this approximation only reduces the dip a little (see fig. 4.16).

In order to show an example of the difference between the equation set from table 4.9 and the more accurate equation set from table 4.10 the transconductance curves shown in fig. 4.15. and fig. 4.16. are calculated for the same DMOST. The difference is mainly determined by δ_1, which can differ from zero considerably for high doping concentrations.

4.5. Conclusion

Although, the DMOST has been proposed to reveal a better linearity owing to the velocity saturation effects of the short channel, its behaviour is determined by the total channellength for gate voltages above a characteristic value, called the transition gate voltage. Due to this effect the transconductance curve shows a dip for those gate voltages at which a high linearity was expected.
To minimize this unwanted dip , there must be a large threshold voltage difference between the two channel regions. Since the doping concentrations of the two regions cannot be varied arbitrarely in practice, the threshold voltage difference is limited. Another aspect for reducing the dip is limitation of the difference between the two channel-lengths. An optimum can be found when the first channellength is almost as long as the second. Since we want the first channel to be shorter, in order to take advantage of velocity saturation effects, the total length of the DMOST must be shorter as well. Unfortunately the minimum total length is limited by the photolithographic process in a standard technology.
Thus, the first thought, that the linearity can be improved arbritarily, by shortening the first channel of the DMOST untill other short channel effects appear, is wrong. Due to normal MOST operation effects the improvement of the linearity by applying DMOSTs,is limited.

5. The depletion MOST

5.1. Introduction

It is shown that a DMOST can offer a better linearity and a higher transconductance, by velocity saturation effects of the first channel. This is only the case if a gate voltage is applied below a characteristic value, called the transition gate voltage [3]. If the gate voltage exceeds this value, the transconductance is determined by both channels, and the short channel properties are lost. Even more, the transconductance curve can show a dip for values of the gate voltage just above the transition gate voltage, which results in nonlinearities. In the previous chapter it is shown that the transition gate voltage can be increased, while the dip flattens, by reducing the difference between the first and second channel length and/or increasing the difference in threshold voltage, where the threshold voltage of the first channel has to be the highest one*. The first possibility has the disadvantage that the minimal first channel length is limited by the total length of the structure. And the minimum of the total length is limited by the photolithographic process. The second possibility, however, seems to be limited by the maximum difference in doping concentrations between both channel regions.However, by applying an N-surface layer the threshold voltage difference may be further increased. While the threshold voltage for P-type silicon is positive, with respect to the flat-band

* This is the case for n-channel DMOSTs. In practice the first channel always is formed by a boron diffusion, due to technological considerations, so only n-channel DMOSTs have our interests, apart from the higher mobility for electrons, compared to the hole mobility.

voltage, now a negative value is found for the second channel region. At zero applied gate voltage the channel is formed by the majority carriers (electrons). The gate voltage has to be negative to deplete this N^+-layer so that the conducting channel disappears. That is why an n-channel MOST with N-surface layer is called a depletion MOST.
Because of the fact that the conductance is provided by majority carriers and moreover the surface layer forms a p-n junction with the bulk, this structure needs a more complicated derivation. In this chapter the main properties of the depletion MOST will be derived, and in the last subsection the results will be applied to DMOSTs with an N-surface layer for the second channel region.

5.2. Channel modes of a depletion MOST

The structure that we consider is shown in fig. 5.1. To evaluate the basic device characteristics it is necessary to know how the channel is formed.

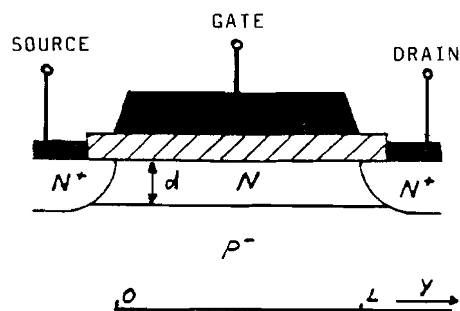

Fig. 5.1. Schematic diagram of a depletion MOST.

In order to deduce this we assume both the drain and the source to be grounded, while they are internally connected by a conducting channel in the N-layer. Under the different gate and bulk bias conditions the

channel potential remains zero volts. If, by zero volts gate bias a negative bulk potential is applied (the p-n junction will always be reverse biased) the N-layer is depleted at the junction side. The channel conductance is provided by the electrons in the neutral part of the N-layer, which will be narrower if a more negative bulk potential is applied. Now one can also apply a negative potential at the gate, which results in a depletion at the surface side. The conducting channel is pushed away from the surface and exists only in the bulk, this will be called the bulk channel. The gate voltage at which the surface depletion region contacts the bulk depletion region is defined as the threshold voltage.
Below this voltage there is no conducting channel between source and drain. It is clear that the threshold voltage is dependent on the bulk potential. On the other hand, if a positive gate voltage is applied, accumulation of electrons at the surface occurs. The conductance is provided by this accumulation charge and by the electrons in the neutral part of the N-layer. This is called the twin channel mode [6]. If in this situation the bulk potential is decreased, it is possible to deplete the whole N-layer, so only surface charge is left. This is called the surface channel mode. The same considerations hold for an arbitrary channel potential, provided that this potential is taken as the reference. If a positive drain potential is applied (by keeping the source grounded), a channel potential distribution arises. In every cross-section of the structure, the channel mode can be derived, by taking the local channel potential as a reference.

5.3. Bulk channel mode

When both the gate and the bulk are negatively biased with respect to the local channel potential V(y) the channel is confined between two depletion regions.

The N-layer is neutral outside the depletion boundaries. (Shockley's depletion approximation) and the channel charge concentration is equal to the doping concentration of the N-layer. Furthermore the transversal electric field at the boundaries in the semiconductor of the depletion regions is zero (see fig. 5.2).

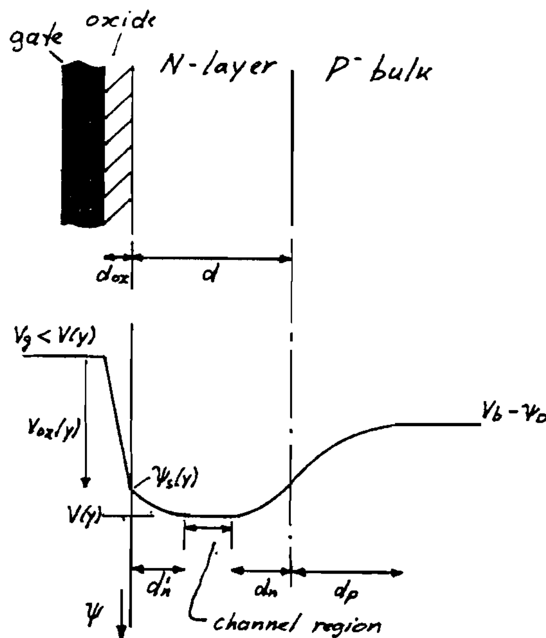

Fig. 5.2. Transversal potential distribution when the gate is negatively biased with respect to the channel. It is seen that the channel region is neutral and the transversal electric field at its boundaries equals zero.

By solving the one-dimensional Poisson equation it follows that :

$$d_n = \sqrt{\frac{2\varepsilon_s N_A}{q N_D (N_A + N_D)}} \sqrt{V(y) - V_b + \psi_D} \qquad [5.1]$$

$$d_n' = \sqrt{\frac{2\varepsilon_s}{q N_D}} \sqrt{V(y) - \psi_s(y)} \qquad [5.3]$$

$$Q_g = C_{ox}(V_g - \psi_s(y)) = -\sqrt{2\varepsilon_s q N_D} \sqrt{V(y) - \psi_s(y)} \qquad [5.3]$$

where d_n is the depletion width in the N-layer at the junction side and d_n' is the depletion width at the surface and d_p is the depletion width in the P^--bulk. The channel charge per unit area can be found with

$$Q_n = -(d - d_n - d_n')\, q\, N_D \qquad [5.4]$$

where d is the width of the N-layer.

$$Q_n = -C_{ox}\left\{\frac{q\,d\,N_D}{C_{ox}} - K_{pn}\sqrt{V(y) - V_b + \psi_D} - \frac{K_n^2}{2}\left[-1 + \sqrt{1 + \frac{4}{K_n^2}(V(y) - V_g)}\right]\right\} \qquad [5.5]$$

with $$K_n = \frac{\sqrt{2\varepsilon_s q N_D}}{C_{ox}} \qquad [5.6]$$

and $$K_{pn} = \frac{\sqrt{2\varepsilon_s q\, N_A N_D/(N_A + N_D)}}{C_{ox}} \qquad [5.7]$$

The threshold voltage V_{tN} follows from Eq. [5.5] by setting $Q_n = 0$ and $V(y) = V_s = 0$

$$V_{tN} = \frac{-1}{K_n^2}\left[\frac{q\,d\,N_D}{C_{ox}} - K_{pn}\sqrt{-V_b + \psi_D}\right]\left[\frac{q\,d\,N_D}{C_{ox}} + K_n^2 - K_{pn}\sqrt{-V_b + \psi_D}\right] \qquad [5.8]$$

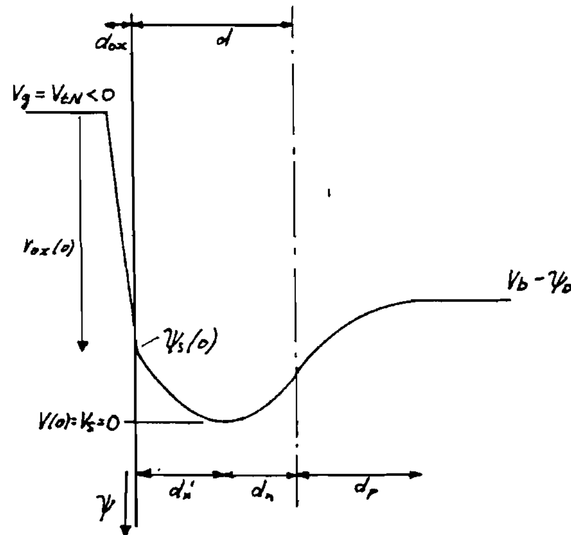

Fig. 5.3. Transversal potential distribution at the source for $V_g = V_{tN}$.

In fig. 5.3 it can be seen that at an increase of the bulk bias (V_b more negative) d_n increases, so d_n' decreases and finally the threshold voltage appears to be less negative. This is in agreement with Eq. [5.8]. It is assumed that $|\psi_s(y)| < |V_b|$ because, otherwise, inversion occurs (holes are attracted from the bulk at the outer ends along the N-layer). When $\psi_s(y) = V_b$ the depletion width has reached its maximum, and there remains a conducting bulk channel, even if the gate voltage is decreased further. This means that the thickness of the N-layer is limited, or a larger bulk bias has to be applied, if it is desired that the channel disappears for $V_g < V_{tN}$. If a negative gate voltage is applied higher than the threshold voltage V_{tN}, there is a bulk channel from the source to the drain. This is visualized in fig. 5.4.

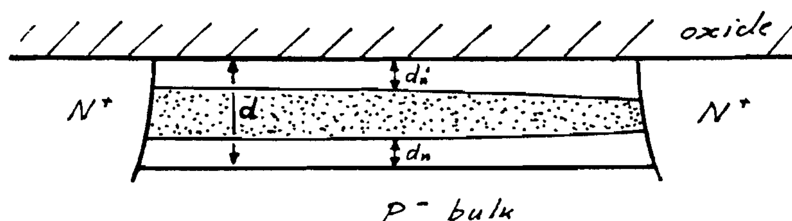

Fig. 5.4. Schematic diagram of a bulk channel.

The pinch off drain voltage can be found from Eq. [5.5] by setting $Q_n = 0$ (if velocity saturation is not taken into account) and $V(y) = V_{dsat}$.

5.4. Twin channel mode

If the gate voltage equals the local channel potential V(y) the bulk channel touches the surface, and when the gate voltage is increased accumulation occurs. The surface potential $\psi_s(y)$ is equal to the channel potential V(y). (see fig. 5.5).

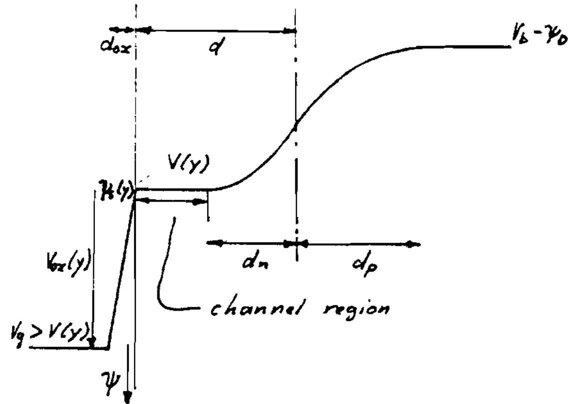

Fig. 5.5. Transversal potential distribution when the gate is positively biased with respect to the channel.
The potential across the oxide is only determined by the accumulation charge at the semiconductor surface.

The conductance is provided by the bulk charge as well as the accumulation charge, so

$$Q_n(y) = -(d-d_n)qN_D - (V_g - V(y))C_{ox} \qquad [5.9]$$

$$= -C_{ox}\left\{\frac{qdN_D}{C_{ox}} - K_{pn}\sqrt{V(y)-V_b+\psi_D} + (V_g - V(y))\right\} \qquad [5.10]$$

where d_n is given by Eq. [5.1]. If the gate is at a higher potential than the drain, there is a twin channel from the source to the drain. This is visualized in fig. 5.6.

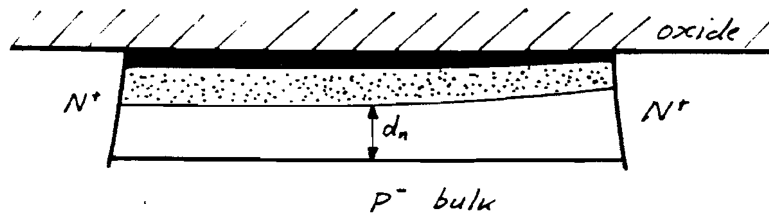

Fig. 5.6. Schematic diagram of a twin channel.

It is assumed that a small bulk bias is applied, so that not the whole N-layer is depleted $(d_n < d)$.

5.5. Surface channel mode

If the channel to bulk potential increases, the depletion width in the N-layer increases until the whole N-layer is depleted $(d_n = d)$ and only a surface channel exists (see fig. 5.7).

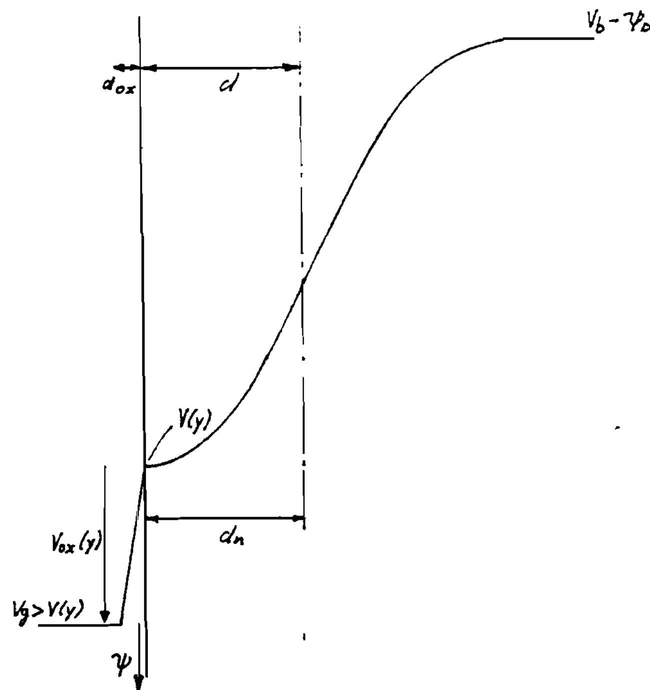

Fig. 5.7. Transversal potential distribution with the same gate to channel potential as in Fig. 5.5. The bulk potential is decreased until the whole N-layer is depleted. The potential across the oxide is still determined by the accumulation charge at the semiconductor surface.

If the bulk potential decreases, while the channel potential remains constant, only the depletion width in the P^- bulk increases. Because the voltage drop across the oxide remains constant in this situation, it is required for charge neutrality that the channel charge decreases with the same amount as the depletion charge increases.

The equation for the channel charge is rather cumbersome, but we can neglect the excess charge deep in the bulk with respect to the total surface channel charge, so

$$Q_n(y) \approx -C_{ox}\{V_g - V(y)\} \qquad [5.11]$$

The value of the channel to bulk potential at which this situation starts, follows from

$$\frac{q\,d N_D}{C_{ox}} = \frac{q\,d_p N_A}{C_{ox}} = K_{pn}\sqrt{V(y)-V_b+\psi_0}$$

$$V(y)-V_b = -\psi_0 + \left(\frac{q\,d N_D}{C_{ox}K_{pn}}\right)^2 \qquad [5.12]$$

5.6. The basic device characteristics

For the different channel modes the drain current can be evaluated. The potential across an elementary section (dy) is given by

$$dV = \frac{I\,dy}{W\mu_n|Q_n(y)|} \qquad [3.11]$$

$$\text{where} \qquad \mu_n = \frac{\mu_0}{1+\frac{dV(y)}{dy}/E_c} \qquad [3.35]$$

if velocity saturation is taken into account. Although the low field mobility of the electrons in the bulk is approximately twice as much as at the surface, due to irregularities at the surface [5] , it will be assumed to be equal for all channel modes. The drain current can be derived by substitution of the channel charge equation which is valid in a particular region into Eq. [3.11] and integrating over this region in a similar way as shown in Appendix A. Besides the different modes, also different combinations of modes are possible. First the single mode drain current equations will be derived, later

some combinations will be discussed. In all situations the MOST is assumed to operate in the triode region. At the end the saturated MOST will be considered.

Bulk channel

When $V_{tN} < V_g \leq 0$ there is only a bulk channel from the source to the drain. Substitution of Eq. [5.5] into Eq. [3.11] yields

$$I_{d\,bulk} = \frac{\beta'}{E_c L + V_d} \left\{ \frac{K_n^2}{2} V_d + \frac{q d N_D}{C_{ox}} V_d - \frac{2}{3} K_n \left[\left(V_d + \frac{K_n}{2} - V_g\right)^{3/2} - \left(\frac{K_n}{2} - V_g\right)^{3/2} \right] - \frac{2}{3} K_{pn} \left[\left(V_d - V_b + \psi_D\right)^{3/2} - \left(-V_b - \psi_D\right)^{3/2} \right] \right\} \quad [5.13]$$

if $V_{tN} < V_g \leq 0$

Twin channel

The condition for a twin channel is that the gate is positively biased with respect to the whole channel. So $V_g > V_d$. At this condition a surface channel is also possible at large bulk bias. To prevent this, a second condition is obtained by Eq. [5.12].

$$-V_b \leq -V_d - \psi_D + \left(\frac{q d N_D}{C_{ox} K_{pn}}\right)^2$$

Substitution of Eq. [5.10] into Eq. [3.11] yields

$$I_{d\,twin} = \frac{\beta'}{E_c L + V_d} \left\{ \left(V_g + \frac{q d N_D}{C_{ox}}\right) V_d - \frac{V_d^2}{2} - \frac{2}{3} K_{pn} \left[\left(V_d - V_b + \psi_D\right)^{3/2} - \left(-V_b + \psi_D\right)^{3/2} \right] \right\} \quad [5.14]$$

if $V_g \geq V_d$ and $-V_b \leq -V_d + \left(\frac{q d N_D}{C_{ox} K_{pn}}\right)^2$

It strucks immediately that this equation shows great similarity with the drain current equation for the ordinary inversion MOST (Eq. [3.40]).

Surface channel

From the previous situation it can be seen that the twin channel mode results in a surface channelmode if the applied bulk bias is increased to

$$-V_b \geq 0 - \psi_D + \left(\frac{q\,d\,N_D}{C_{ox}\,K_{pn}}\right)^2 \qquad (id.\ V_s = 0)$$

In this situation the channel charge is given by Eq. [5.11]. This yields

$$I_{d\,surf} = \beta' \, \frac{V_g V_d - \frac{V_d^2}{2}}{E_c L + V_d}$$

$$\text{if } V_g > V_d \text{ and } -V_b \geq -\psi_D + \left(\frac{q\,d\,N_D}{C_{ox}\,K_{pn}}\right)^2 \qquad [5.15]$$

It is seen that the dependancy of the bulk charge is lost. This is due to the approximation in Eq. [5.11]. Eq. [5.15] is similar to the drain current for the inversion MOST given by Eq. [3.41].

Twin channel + surface channel

If a bulk voltage between the previous boundaries is applied,

$$-V_d - \psi_D + \left(\frac{q\,d\,N_D}{C_{ox}\,K_{pn}}\right)^2 < -V_b < -\psi_D + \left(\frac{q\,d\,N_D}{C_{ox}\,K_{pn}}\right)^2$$

the channel will be devided in two regions. In the first region, at the source side, a twin channel exists, and in the second region, at the drain side only a surface channel exists (see fig. 5.8) for $V_g > V_d$.

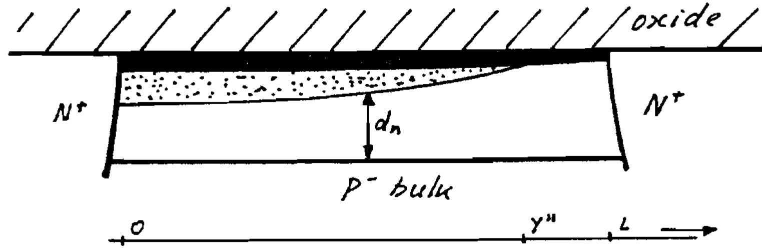

Fig. 5.8. Schematic diagram of a twin + surface channel.

The potential at the transition point y'' between the twin channel region and the surface channel region follows from Eq. [5.12]

$$V(y'') = V_b - \Psi_D + \left(\frac{q\,d N_D}{C_{ox} K_{pn}}\right)^2$$

The drain current can be obtained by a similar method as shown in the next channel mode combination.

Twin channel + bulk channel

If a gate voltage between 0 and V_d is applied, the channel potential equals V_g at $y = y'$. Between the source and this point the channel potential is negative with respect to the gate and a twin channel is formed. From the point y' to the drain, the channel potential is positive with respect to the gate, so a bulk channel exists in that region (see fig. 5.9).

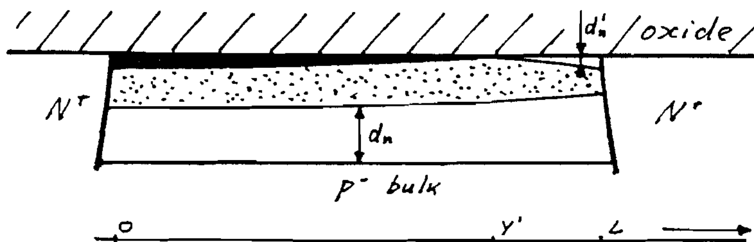

Fig. 5.9. Schematic diagram of a twin + bulk channel.

At a decrease of the gate voltage the point y' shifts towards the source and at an increase of the gate voltage the point shifts towards the drain. Substitution of Eq. [5.10] into Eq. [3.11] and integration from the source ($y = 0$, $V(0) = 0$) to the point y' ($y = y'$, $V(y') = V_g$), followed by substitution of Eq. [5.5] into Eq. [3.11] and integration from the point y' to the drain ($y = L$, $V(L) = V_d$) yields

$$I_{d\,twin+bulk} = \frac{\beta'}{E_c L + V_d} \left\{ \frac{K_n^2}{2}(V_d - V_g) + \frac{q d N_D}{C_{ox}} + \frac{V_g^2}{2} - \frac{2}{3} K_n \left[\left(V_d + \frac{K_n}{2} - V_g\right)^{3/2} - \left(\frac{K_n}{2} - V_g\right)^{3/2} \right] - \frac{2}{3} K_{pn} \left[(V_d - V_b + \psi_D)^{3/2} - (-V_b + \psi_D)^{3/2} \right] \right\} \quad [5.16]$$

if $0 \leq V_g \leq V_d$

For $V_g = 0$ this equation results in the equation for the bulk-mode (Eq. [5.13] where $V_g = 0$) and for $V_g = V_d$ the equation for the twinmode (Eq. [5.14] where $V_g = V_d$) will be obtained.

As said before, the drain current equation for the twin channel mode (Eq. [5.14]) shows great similarity with the drain current equation (Eq. [3.40]). This is due to the fact that the channel is formed by a surface channel, just as at an inversion MOST, and formed by a region in the bulk, which touches the surface, comparable with the depletion region in an inversion MOST.
If we take two terms of the Taylor expansion of $(V_d + \psi_D - V_b)^{3/2}$ into account, Eq. [5.14] can be approximated by

$$I_{d\,twin} = \beta' \frac{(V_g - V_{tA})V_d - V_d^2/2}{E_c L + V_d} \quad [5.17]$$

with $$V_{tA} = -\frac{q d N_D}{C_{ox}} + K_n \sqrt{-V_b + \psi_D} \quad [5.18]$$

It should be noticed that V_{tA} is not the threshold voltage

of the depletion MOST. It is an apparent threshold voltage because it shows a mathematical similarity with the threshold voltage of an inversion MOST. Moreover, this voltage can only be measured indirectly from the characteristics of a depletion MOST. If we compare Eq. [5.17] and Eq. [5.15] it is seen that besides V_{tA} both equations are equal. Eq. [5.17] holds for the twin channel mode, and Eq. [5.15] holds for the surface channel mode. The difference between these modes is caused by the bulk bias.
It was seen that if

$$-V_b \leq -V_d - \psi_D + \left(\frac{q\, d N_D}{C_{ox} K_{pn}}\right)^2$$

there is the twin channel mode, and Eq. [5.14] holds, which is approximated by Eq. [5.17].
When the bulk bias is increased to

$$-V_b > -V_d - \psi_D + \left(\frac{q\, d N_D}{C_{ox} K_{pn}}\right)^2 \quad \text{but} \quad -V_b < -\psi_D + \left(\frac{q\, d N_D}{C_{ox} K_{pn}}\right)^2$$

there is the twin + surface channel mode, for which we did not derive the drain current equation. If, finally, the bulk bias is increased to

$$-V_b \geq -\psi_D + \left(\frac{q\, d N_D}{C_{ox} K_{pn}}\right)^2$$

there is the surface channel mode and Eq. [5.15] holds. But Eq. [5.17] results in Eq. [5.15] if $-V_b = -\psi_D + \left(\frac{q\, d N_D}{C_{ox} K_{pn}}\right)^2$ because at this bulk bias $V_{tA} = 0$
Thus, by the increase of the bulk bias from zero until $-\psi_D + \left(\frac{q\, d N_D}{C_{ox} K_{pn}}\right)^2$ first the MOST is in the twin channel mode, next in the twin + surface channel mode and finally in the surface channel mode. And it is seen that the approximated equation for the twin channel mode results in the equation for the surface channel mode at increasing the bulk bias. So, it is reasonable to assume that the approximated equation also holds for the twin + surface channel mode.

Thus the drain current for the twin channel, twin + surface channel and the surface channel mode is given by

$$I_d = \beta' \frac{(V_g - V_{tA})V_d - V_d^2/2}{E_c L + V_d}$$

$$\text{where} \quad V_{tA} = -\frac{q d N_D}{C_{ox}} + K_{pn}\sqrt{-V_b + \psi_b} \quad \text{if } -V_b \leq -\psi_b + \left(\frac{q d N_D}{C_{ox} K_{pn}}\right)^2 \qquad [5.19]$$

$$\text{and} \quad V_{tA} = 0 \qquad \text{if } -V_b \geq -\psi_b + \left(\frac{q d N_D}{C_{ox} K_{pn}}\right)^2$$

Eq. [5.13] and Eq. [5.16] are essentially different from Eq. [5.14] and they cannot easily be approximated by a simple equation. Because it is unpractical to describe the drain current for the three different modes with three different equations, we will try to use Eq. [5.19] for all channel modes, as long as the MOST operates in the triode region. Fig. 5.10 shows the drain current versus drain voltage, with the gate voltage as parameter, calculated from the "exact" equations (Eq. [5.13], Eq.[5.14], Eq. [5.15], Eq. [5.16]) (solid curves) and calculated with the approximated equation Eq. [5.19] (dashed curves).

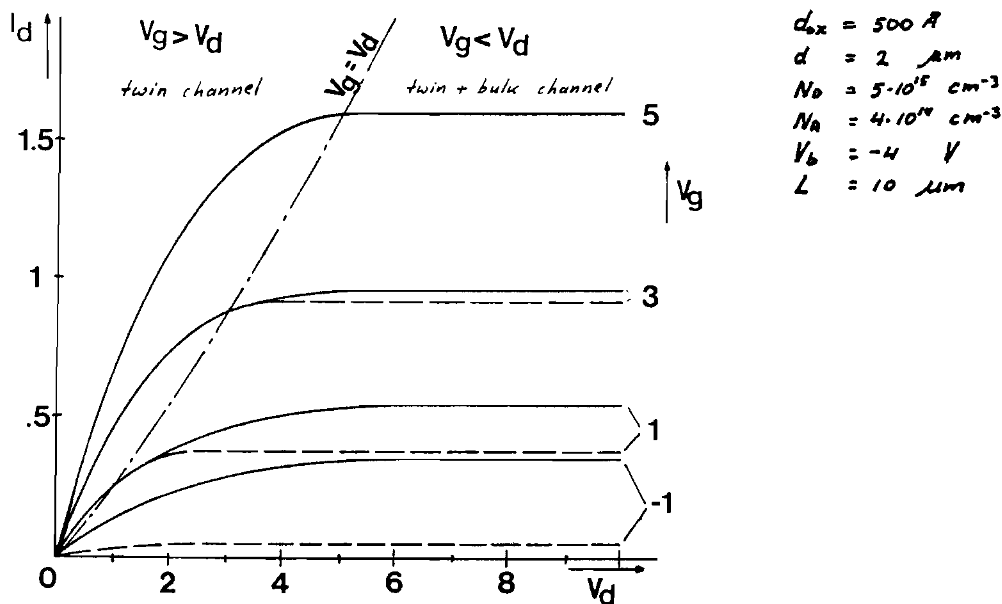

Fig. 5.10. Comparison of the exact drain current curves (solid curves) with the approximated drain current curves (dashed curves), of a depletion MOST.

For the exact curves as well as the approximated curves it is assumed that saturation occurs when the drain current reaches its maximum.
As can be seen for $V_g > V_d$ the approximation is excellent. For $0 < V_g < V_d$ the approximation is rather good, especially in the upper part of this range. This can be explained by the following considerations. The longitudinal channel potential increases progressive towards the drain. This means that, for the main part of the channel, the channel potential is negative with respect to the gate. In other words, the point y' is near the drain, even for relatively small gate voltages. So the main part of the channel is formed by a twin channel, and only a small part of the channel, near the drain, is formed by a bulk channel. For the twin channel region the approximation holds, but an error is introduced by the bulk channel region. As long as the bulk channel region is relatively small, the error is small. For very small values of the gate voltage the error becomes more important. When $V_g < 0$, only a bulk channel exists and the approximation fails completely. This last is also due to the difference between the real threshold voltage V_{tN} and V_{tA}, where always $V_{tN} < V_{tA}$. This will be shown in the next subsection. The approximation predicts that for $V_g < V_{tA}$ no currents can flow. In practice, however, this is true for $V_g < V_{tN}$, Even for thick N-layers and/or low bulk bias, there always remains a conducting channel as a result of a shielding inversion layer. Therefore, we will use Eq. [5.19] under the condition that $V_g > 0$, or in general $V_g > V_s$.
In conclusion we can describe the drain current in the triode region of the depletion MOST by

$$I_d = \frac{(V_g - V_{tA}) V_d - V_d^2/2}{E_c L + V_d} \qquad \text{for } V_g > 0$$

[5.20]

$$\text{where } V_{tA} = -\frac{q d N_D}{C_{ox}} + K_{pn}\sqrt{-V_b + \psi_b} \qquad \text{if } -V_b \leq -\psi_b + \left(\frac{q d N_D}{C_{ox} K_{pn}}\right)^2$$

$$\text{and } V_{tA} = 0 \qquad \text{if } -V_b \geq -\psi_b + \left(\frac{q d N_D}{C_{ox} K_{pn}}\right)^2$$

and by Eq. [5.13] for $V_{tN} < V_g \leq 0$.
From now on we will only consider the case for $V_g > 0$.
At the saturation drain voltage the drain current reaches its maximum and can be derived from $\frac{\partial I_d}{\partial V_d} = 0$

$$I_{dsat} = \beta' (V_g - V_{tA} - V_{dsat})$$

$$V_{dsat} = E_c L \left\{ -1 + \sqrt{1 + \frac{V_g - V_{tA}}{E_c L}} \right\}$$

5.7. Derivation of the apparent threshold voltage V_{tA}

In contrast with an inversion MOST, where the threshold voltage V_t in the drain current equation agrees with the gate voltage at which channel conduction starts, the real threshold voltage V_{tN} of a depletion MOST is essential different from the apparent threshold voltage V_{tA} in the drain current equation, Eq. [5.20]. If the drain current equation is used, the apparent threshold voltage V_{tA} should be known. Now it will be shown that it is possible to derive V_{tA} from V_{tN}.
Consider both threshold voltage equations :

$$V_{tA} = 0 \qquad \text{if } -V_b \geq -\psi_D + \left(\frac{q d N_D}{C_{ox} K_{pn}}\right)^2$$

$$V_{tA} = -\frac{q d N_D}{C_{ox}} + K_{pn}\sqrt{-V_b + \psi_D} \qquad \text{if } -V_b \leq -\psi_D + \left(\frac{q d N_D}{C_{ox} K_{pn}}\right)^2 \qquad [5.21]$$

$$V_{tN} = \frac{-1}{K_n^2}\left[\frac{q d N_D}{C_{ox}} - K_{pn}\sqrt{-V_b + \psi_D}\right]\left[\frac{q d N_D}{C_{ox}} + K_n^2 - K_{pn}\sqrt{-V_b + \psi_D}\right] \qquad [5.8]$$

If $q d N_D / C_{ox} K_{pn}$ is known we can distinguish the different cases for $-V_b$ in Eq. [5.21]. At this moment this is unknown, therefore assume that $-V_b \leq -\psi_D + \left(\frac{q d N_D}{C_{ox} K_{pn}}\right)^2$ and substitute Eq. [5.21] into Eq. [5.8]:

$$V_{tN} = \frac{-1}{K_n^2}\left[-V_{tA}\right]\left[K_n^2 - V_{tA}\right]$$

$$\text{or} \quad V_{tA} = \frac{K_n^2}{2}\left[1 - \sqrt{1 - \frac{4V_{tN}}{K_n^2}}\right] \qquad [5.22]$$

Only the minus sign holds because V_{tA} is negative.
If the bulk factor K_n is known we can calcualte V_{tA}, because V_{tN} can be measured for every structure if an appropriate bulk bias is applied.
Eq. [5.8] can be written as

$$V_{tN} = \frac{K_{pn}^2}{K_n^2}\left(-V_b + \psi_b\right) - K_{pn}\left(1 + 2\frac{q\,d\,N_D}{C_{ox}K_n^2}\right)\sqrt{-V_b+\psi_b} + \left(\frac{q\,d\,N_D}{C_{ox}K_n}\right)^2 + \frac{q\,d\,N_D}{C_{ox}} \qquad [5.23]$$

$$\text{or} \quad V_{tN}(-V_b) = \alpha\left(-V_b + \psi_D\right) - \beta\sqrt{-V_b + \psi_D} + \gamma$$

where $\alpha = K_{pn}^2 / K_n^2$

$$\beta = K_{pn}\left(1 + 2\frac{q\,d\,N_D}{C_{ox}K_n^2}\right)$$

$$\gamma = \frac{q\,d\,N_D}{C_{ox}}\left(1 + \frac{q\,d\,N_D}{C_{ox}K_n^2}\right)$$

The curve V_{tN} versus $-V_b$ can be obtained by measurement of the threshold voltage V_{tN} at different values of the bulk bias. If these values are not too small, the estimation for ψ_D will not introduce an error. The coefficients, α, β and γ can be obtained by deriving the curve with the method of least squares. When the coefficients α, β and γ are known the bulk factor K_n can be derived (see Appendix E) as well as $q\,d\,N_D / C_{ox}K_{pn}$

$$K_n = \sqrt{\frac{\beta^2}{\alpha} - 4\gamma} \qquad [5.24]$$

$$\frac{q\,d\,N_D}{C_{ox}K_{pn}} = \frac{\beta}{2\alpha}\left[1 - \sqrt{1 - \frac{4\alpha\gamma}{\beta^2}}\right]$$

It is noticed that small errors in the coefficients α, β and γ results in a relatively large error in K_n, because the values of the terms β^2/α and 4γ are almost equal for small K_n, and the values of the separate terms are much larger than their subtraction.
Fig. 5.11 shows the apparent threshold voltage V_{tA} versus the real threshold voltage V_{tN}, with the bulk factor K_n as parameter.

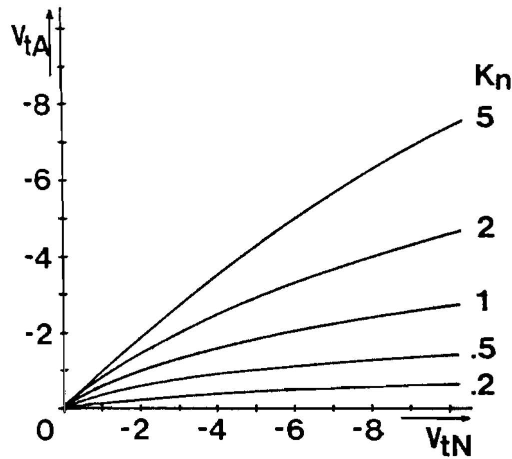

Fig. 5.11.The apparent threshold voltage V_{tA} vs the real threshold voltage V_{tN} with K_n as parameter.

It is seen that for a large bulk factor K_n the apparent threshold voltage approaches the real threshold voltage.
For small K_n, however, V_{tA} is considerable smaller than V_{tN}.
The difference between V_{tA} and V_{tN} is caused by the fact that V_{tA} is used in the drain current equation which holds for channels at the surface, while V_{tN} is the threshold voltage for the channel which starts in the bulk.
As concluded in subsection 5.3., when $\psi_s(y)=V_b$ inversion at the surface occurs, because holes are attracted from the bulk at the outer ends along the N-layer.
When there is a channel for $\psi_s(y) = V_b$, it cannot be pinched off by decreasing the gate voltage, because the

surface depletion width has reached its maximum. This means that for a given N-layer thickness there is a value for the bulk bias at which, for a proper gate voltage, just inversion starts when the depletion region at the surface touches the depletion region at the junction. This bulk bias can be found by summation of Eq. [5.1] and Eq. [5.2] where $\psi(0) = V_s = 0$, $\psi_s(0) = V_b$ and $d_n + d_n' = d$.

$$\frac{q d N_A}{C_{ox}} = K_{pn}\sqrt{-V_b + \psi_D} + K_n\sqrt{-V_b}$$

The solution can be approximated by ($\psi_D \ll -V_b$)

$$V_{bmin} \approx -\left(\frac{q d N_A / C_{ox}}{K_{pn} + K_n}\right)^2 = -\left(\frac{q d N_A}{\sqrt{2\varepsilon_s q N_A N_D/(N_A + N_D)} + \sqrt{2\varepsilon_s q N_A}}\right)^2$$

The value of the threshold voltage at this bulk bias can be found by deriving the potential across the oxide

$$V_{tNmin} = -V_{bmin} - K_n\sqrt{-V_{bmin}}$$

The subscribt "min" is used because this is the minimal value for the threshold voltage at a given device geometry and given doping concentrations. Thus for $V_b > V_{bmin}$ inversion occurs before the channel is pinched off at decreasing gate voltage, so no threshold voltage exists. When the threshold voltage does not exist, the comparison of V_{tA} with V_{tN} in fig. 5.11, is meaningless, but the apparent threshold voltage V_{tA} is still the correct parameter for deriving the drain current by Eq. [5.20] .

5.8. The DMOST with N-surface layer

The structure is shown in fig. 5.12. The N-layer is implanted in the whole MOST region, before the gate is formed. The first channel is formed with an overdope of

acceptors. This means that the doping concentration of the N-layer is limited.

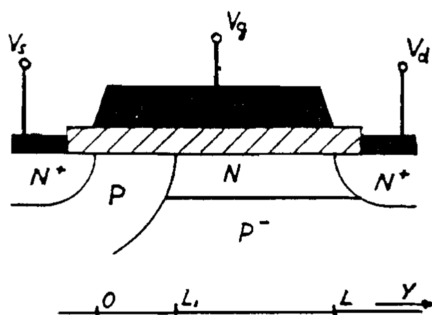

Fig. 5.12.Schematic diagram of a DMOST with N-layer.

Only the net doping is taken into account.
The equations for the drain current and transconductance of a DMOST without the N-layer are derived in chapter 4. As can be seen from Eq. [5.20] the equations of the ordinary DMOST hold for a DMOST with N-layer if the apparent threshold voltage is used and as long as $V_g > V_c$ (because the source potential of the second MOST is the common potential V_c).
When $V_g \leq V_c$ the drain current is given by Eq. [5.13], which nature completely differs from the equations for which the DMOST formulas are derived. Now, it will be shown that this is not a problem at all.
Consider the longitudinal potential distribution of the DMOST with N-layer at the transition gate voltage V_{gT} (see fig. 5.13).

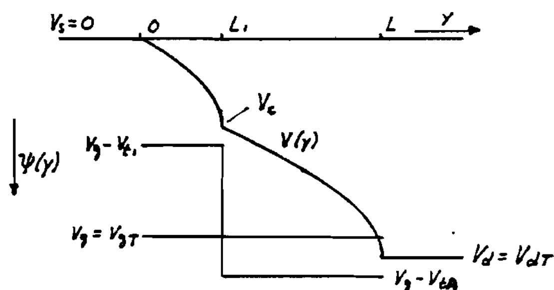

Fig. 5.13.Longitudinal potential distribution for a DMOST with N-layer at the transition gate voltage V_{gT}.

In this situation it is obvious that $V_g > V_c$ because the threshold voltage of the first channel is positive.
If $V_g > V_{gT}$ it can be seen in fig. 4.4. that the condition $V_g > V_c$ still holds.
If $V_g < V_{gT}$, however, it is seen in fig. 4.5b, c that the condition $V_g > V_c$ no longer holds. But, as we know, in this situation the drain current is completely determined by the first channel !!!
So the equation set of fig. (4.9.) holds for the DMOST under any biasing condition, where the difference in threshold voltage is given by

$$\Delta V_t = V_{t1} - V_{tA} \qquad [5.25.]$$

Furthermore it is seen from fig. 5.13. that always $V_g > V_c + V_T$ when the drain current is also determined by the second channel region. It was required that $V_g > V_c$ (see page 66), so this means that Eq. [5.20] is a very good approximation, when it is used for DMOST calculations.

5.9. Conclusions

To improve the linearity of a DMOST, a large threshold voltage difference between the two channel regions is desired. This can be achieved by forming an N-layer at the surface of the second channel region. The threshold voltage of this region is negative and should be minimized. One would expect that this can be achieved with thick highly doped N-layers, where a large bulk bias is applied. However, this is limited by the breakdown voltage for the p-n junction in the bulk. When a sufficient small bulk bias is applied, inversion occurs at a decrease of the gate voltage before the channel is pinched off. Holes are attracted from the bulk at the outer ends along the N-layer, and they have a shielding effect on the gate. In this situation, there exists no threshold voltage at all.
The threshold voltage difference, which determines the behaviour of the DMOST with N-layer, however, is not the difference between the threshold voltage of the first channel and the

real threshold voltage of the second channel, but the difference between the threshold voltage of the first channel and an apparent threshold voltage of the second channel.
This apparent threshold voltage is always less negative as the real threshold voltage. This means that the effective threshold voltage difference is less than expected.
For large values of the bulk factor of the N-layer (K_n>5) the apparent threshold voltage approaches the real threshold voltage, when it exists.
Minimization of the apparent threshold voltage is limited by the same causes as those for the real threshold voltage.
Because the oxide capacitance should be large to obtain a large gainfactor $\beta' = W v_{sat} C_{ox}$, the bulkfactor is relatively small. In practice this means that the apparent threshold voltage is considerably less negative as the real threshold voltage. So the threshold voltage difference as well as the improvement of the linearity are less strongly marked as expected.

6. The dual gate MOST

6.1. Introduction

The dual gate MOST has just like the DMOST two channel regions. The channel region under the first gate corresponds with the highly P-doped first channel region of the DMOST and the channel region under the second gate corresponds with the low P-doped, or N-doped region of the DMOST. Due to the standard technological processes the channellengths of the dual gate MOST are longer than those of the DMOST. Owing to the similarity, in principle, the DMOST equations can be used for dual gate MOST analysis.

6.2. Transconductance characteristics of the dual gate MOST

Fig. 6.1 shows the comparison of the dual gate MOST with the DMOST.

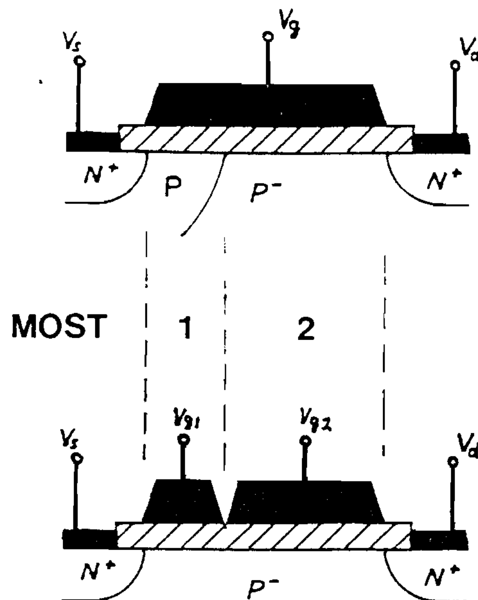

Fig. 6.1. Comparison of a DMOST with a dual gate MOST.

The threshold voltage difference (ΔV_t) of the DMOST corresponds with the difference in the DC-bias of the two gates (ΔV_g). This is understood from the following bias conditions.
The gate voltages of the DMOST are given by :

$V_g - V_{t1} = V_g'$ for the first channel region

$V_g - V_{t2} = V_g' + \Delta V_t$ for the second channel region

$V_{t1} - V_{t2} = \Delta V_t$

which results in the gate voltages of the dual gate MOST

$V_{g1} - V_t = V_{g1}'$ for the first channel region

$V_{g2} - V_t = V_{g2}'$ for the second channel region

$V_{g2} - V_{g1} = \Delta V_g$ [6.1]

So V_g' has to be replaced by V_{g1}' , $V_g' + \Delta V_t$ by V_{g2}' , and ΔV_t by ΔV_g.
The modes of operation can be deduced from the transition gate voltage

$$V_{gT1}' = \frac{(\Delta V_g)^2}{2 E_c L_2} + \Delta V_g \sqrt{\frac{E_c L_1}{E_c L_2}} \qquad [6.2]$$

just like the DMOST. If the gate voltage difference ΔV_g is given, then the dual gate MOST operates in the PT or PP mode for $V_{g1} < V_{gT1}$ and in the TP mode for $V_{g1} > V_{gT1}$.
The transconductance equations can be obtained from table 4.9. For the dual gate MOST we must distinguish three cases for applying signal to the gates, i.e. signal to the first gate only, signal to the second gate only or signal to both gates. For the transconductance in the TP mode, the common voltage V_{c2} must be known. This voltage is dependent on the bias conditions.
V_{c2} can be obtained from table 4.9. by changing the gate voltages proposed in Eq.[6.1].

$$V_{c2} = E_c L_2 + \Delta V_g - \sqrt{(E_c L_2 + \Delta V_g)^2 + 2 E_c L_2 (V'_{g1} - V'_{gT1})} - E_c L_1$$

$$+ \sqrt{\left[E_c L_2 + \Delta V_g - \sqrt{(E_c L_2 + \Delta V_g)^2 + 2 E_c L_2 (V'_{g1} - V'_{gT1})}\right]^2 + \left[E_c L_1 + V'_{g1}\right]^2 - \left[V'_{g1}\right]^2} \qquad [6.3]$$

When the signal is applied to both gates, indicated with (1+2), the transconductance equations are equal to those of the DMOST , if the right gate voltages are substituted. (see fig. 6.2).

$$g_{m(1+2)} = \left.\frac{\partial I_d}{\partial V'_g}\right|_{V_d = const} \quad with \ \partial V'_g = \partial V'_{g1} = \partial V'_{g2}$$

$$g_{mPT(1+2)} = g_{mPP(1+2)} = \beta'\left[1 - \left(1 + 2\frac{V'_{g1}}{E_c L_1}\right)^{-1/2}\right] \qquad [6.4a]$$

$$g_{mTP(1+2)} = \beta'\left(1 - \frac{\partial V_{c2}}{\partial V'_g}\right)\left[1 - \left(1 + 2\frac{V'_{g2} - V_{c2}}{E_c L_2}\right)^{-1/2}\right] \qquad [6.4b]$$

$$\frac{\partial V_{c2}}{\partial V'_g} = \frac{(E_c L_1 + V_{c2})\left(1 + 2\frac{V'_{g2} - V_{c2}}{E_c L_2}\right)^{-1/2} - E_c L_1}{(E_c L_1 + V_{c2})\left(1 + 2\frac{V'_{g2} - V_{c2}}{E_c L_2}\right)^{-1/2} - E_c L_1 + E_c L_2 + \Delta V_g - V_{c2} - E_c L_2\sqrt{1 + 2\frac{V'_{g2} - V_{c2}}{E_c L_2}}} \qquad [6.4c]$$

As concluded in chapter 4, the current of the DMOST in PT or PP mode is completely determined by the first channel. If the signal only is applied to the second gate, the transconductance equals zero in the PT or PP mode.

So,

$$g_{mPT(2)} = g_{mPP(2)} = 0 \qquad [6.5a]$$

In the TP mode the drain current is determined by both channels. The second channel region becomes more important at higher gate voltages, because the transconductance is mainly determined by velocity saturation effects at the drain.

The transconductance in this mode also follows from table 4.9.

$$g_{m(2)} = \left.\frac{\partial I_d}{\partial V'_{g2}}\right|_{V_d = const}$$

$$g_{mTP(2)} = \left(1 - \frac{\partial V_{c2}}{\partial V'_{g2}}\right)\left[1 - \left(1 + 2\,\frac{V'_{g2} - V_{c2}}{E_c L_2}\right)^{-1/2}\right] \qquad [6.5b]$$

$$\frac{\partial V_{c2}}{\partial V'_{g2}} = \frac{(E_c L_1 + V_{c2})\left(1 + 2\,\frac{V'_{g2} - V_{c2}}{E_c L_2}\right)^{-1/2} - E_c L_1 - V_{c2}}{(E_c L_1 + V_{c2})\left(1 + 2\,\frac{V'_{g2} - V_{c2}}{E_c L_2}\right)^{-1/2} - E_c L_1 + E_c L_2 + \Delta V_g - V_{c2} - E_c L_2\sqrt{1 + 2\,\frac{V'_{g2} - V_{c2}}{E_c L_2}}} \qquad [6.5c]$$

Eq. [6.5c] can be obtained by implicit differentiation of the fourth power equation in Appendix D1 (see also Appendix D2).

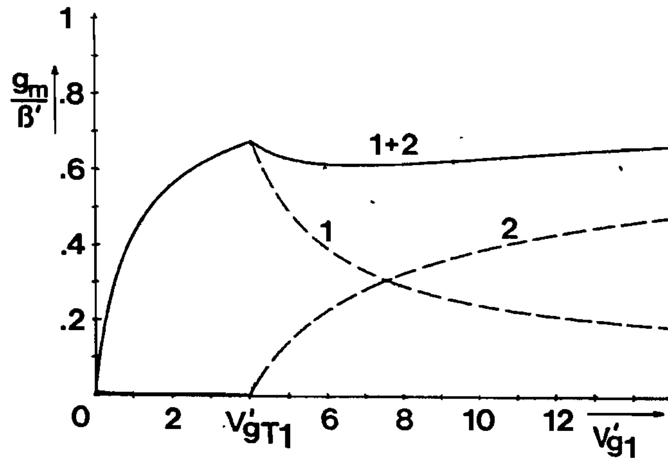

Fig. 6.2. Transconductance vs gate voltage for a saturated dual gate MOST with signal on the first gate only, the second gate only (dashed curves) and on both gates (solid curve).

The transconductance in the PT and PP mode, by applying signal to the first gate only, is equal to the transconductance when the signal is applied to both gates.

$$g_{mPT(1)} = g_{mPP(1)} = \beta'\left[1 - \left(1 + 2\,\frac{V'_{g1}}{E_c L_1}\right)^{-1/2}\right] \qquad [6.6a]$$

In the TP mode the transconductance is then

$$g_{m(1)} = \left.\frac{\partial I_d}{\partial V'_{g1}}\right|_{V_d = const}$$

$$g_{mTP(1)} = -\frac{\partial V_{c2}}{\partial V'_{g1}} \left[1 - \left(1 + 2\,\frac{V'_{g2} - V_{c2}}{E_c L_2}\right)^{-1/2} \right] \qquad [6.6b]$$

$$\frac{\partial V_{c2}}{\partial V'_{g1}} = \frac{V_{c2}}{(E_c L_1 + V_{c2})\left(1 + 2\,\frac{V'_{g2} - V_{c2}}{E_c L_2}\right)^{-1/2} - E_c L_1 + E_c L_2 + \Delta V_g - V_{c2} - E_c L_2 \sqrt{1 + 2\,\frac{V'_{g2} - V_{c2}}{E_c L_2}}} \qquad [6.6c]$$

From Eq. [6.4c], Eq. [6.5c] and Eq. [6.6c] it is seen that

$$\frac{\partial V_{c2}}{\partial V'_g} = \frac{\partial V_{c2}}{\partial V'_{g1}} + \frac{\partial V_{c2}}{\partial V'_{g2}}$$

and for the three modes we obtain

$$g_{m(1+2)} = g_{m(1)} + g_{m(2)}$$

This last is also shown in fig. 6.2.
When two different signals are applied to the gates, it is possible to control their individual transconductance, by varying the gate bias, and keeping the gate bias difference constant. So, the ratio of the mixed output signals can be varied.

6.3. Conclusion

With the dual gate MOST it is possible to improve the linearity by increasing the difference between the gate voltages. On the other hand short channel properties are lost because the minimum channel length of the first channel is longer, due to the photolithographic process in the standard technology.
Furthermore by varying the biasing of the dual gate MOST the influence of the individual gate signals on the drain current can be controlled.

References

1 Sze, S.M., Physics of Semiconductor Devices, John Wiley & Sons, Inc., New York, 1969.

2 Ziel, A. van der, Solid State Physical Electronics, Prentice-Hall, Inc., Englewood Cliffs, New Jersey, 1976.

3 Klaassen, F.M., Review of Physical Models for MOS Transition , Process and Device Modeling for Integrated Circuit Design, Eds. v.d. Wiele, Engl, Jespers, Noordhoff, Leiden, 1977.

4 Rodgers, T.J. et al., An Experimental and Theoretical Analysis of Double-Diffused MOS Transistors, IEEE J. Solid-State Circuits, vol. SC-10, pp. 322-330, Oct. 1975.

5 Fang, F.F. and Fowler, A.B., Hot Electron Effects and Saturation Velocities in Silicon Inversion Layers, J. Appl. Phys., Vol. 41, pp. 1825-1831, March 1970.

6 Esser, L.J.M. and Sangster, F.L.J., Charge Transfer Devices, Handbook on Semiconductors, vol. 4, Vol. Ed. C. Hilsum, Chapter 3B, North-Holland Publishing Company, pp. 325-424, Amsterdam, 1981.

7 Stikvoort, E.F., Increase of gate capacitance in DMOST, IEEE Trans. Electron Device (USA), vol. ED-25, no. 12, pp. 1388-94, Dec. 1978.

8 Lin, Kokalis, Bandy, Modeling of Short Channel MOS Transistors, Electrical Engng. Dept. Univ. of Maryland, College Park, MD, USA Modeling and Simulation, vol. 7, Pittsburgh, PA, USA, 26-27 Apr. 1976, pp. 567-71, 1976.

9 Barsan, R.M., Analysis and Modeling of Dual-Gate MOSFETs, IEEE Trans. Electron Devices, vol. ED-28, no. 5, pp. 523-34, May 1981.

10 Mukherjee, S. Theoretical and Experimental Analysis of Deep Depletion MOSFET, etc., Philips Internal report.

11 Klaassen, F.M., Halfgeleiderelectronica, collegedictaat THE, no. 5.516, Eindhoven 1978.

Appendix A

The voltage drop across an elementary section in the channel is given by

$$dV(y) = \frac{I_d \, dy}{W \mu_n |Q_n(y)|}$$

with

$$Q_n(y) = -\left[V_g - 2\psi_B - V(y)\right] C_{ox} + \sqrt{2 \varepsilon_s q N_A \left[V(y) + 2\psi_B - V_b\right]}$$

$$I_d \, dy = W \mu_n C_{ox} \left\{ \left[V_g - 2\psi_B - V(y)\right] - \frac{\sqrt{2 \varepsilon_s q N_A}}{C_{ox}} \sqrt{V(y) + 2\psi_B - V_b} \right\} dV$$

Integration from the source (y = 0, V = 0) to the drain (y = L, V = V_d) yields

$$\int_0^L I_d \, dy = W \mu_n C_{ox} \int_0^{V_d} \left[V_g - 2\psi_B - V(y) - \frac{\sqrt{2 \varepsilon_s q N_A}}{C_{ox}} \sqrt{V(y) + 2\psi_B - V_b} \right] dV(y)$$

$$I_d L = W \mu_n C_{ox} \left\{ (V_g - 2\psi_B) V_d - \frac{V_d^2}{2} - \frac{2}{3} \frac{\sqrt{2 \varepsilon_s q N_A}}{C_{ox}} \left[(V_d + 2\psi_B - V_b)^{3/2} - (2\psi_B - V_b)^{3/2} \right] \right\}$$

The Taylor expansion of the term $(V_d + 2\psi_B - V_b)^{3/2}$ round V_d = 0 is given by

$$(V_d + 2\psi_B - V_b)^{3/2} = (2\psi_B - V_b)^{3/2} + \frac{3}{2} V_d \sqrt{2\psi_B - V_b} + \frac{1}{2} \cdot \frac{3}{4} \frac{V_d^2}{\sqrt{2\psi_B - V_b}} + \cdots$$

If only two terms are taken into account this leads to

$$I_d = \frac{W \mu_n C_{ox}}{L} \left\{ \left(V_g - 2\psi_B - \frac{\sqrt{2 \varepsilon_s q N_A}}{C_{ox}} \sqrt{2\psi_B - V_b} \right) V_d - \frac{V_d^2}{2} \right\}$$

$$= \beta \left\{ (V_g - V_t) V_d - \frac{V_d^2}{2} \right\}$$

with $\beta = \frac{W \mu_n C_{ox}}{L}$

and $V_t = 2\psi_B + \frac{\sqrt{2\varepsilon_s q N_A}}{C_{ox}} \sqrt{2\psi_B - V_b} = 2\psi_B + K_p \sqrt{2\psi_B - V_b}$

$$K_p = \frac{\sqrt{2\varepsilon_s q N_A}}{C_{ox}}$$

The three term approximation results in

$$I_d = \frac{W \mu_n C_{ox}}{L} \left\{ \left(V_g - 2\psi_B - \frac{\sqrt{2\varepsilon_s q N_A}}{C_{ox}} \sqrt{2\psi_B - V_b} \right) V_d - \left(1 + \frac{\sqrt{2\varepsilon_s q N_A}}{C_{ox}} \cdot \frac{1}{2\sqrt{2\psi_B - V_b}} \right) \frac{V_d^2}{2} \right\}$$

$$= \beta \left\{ (V_g - V_t) V_d - (1 + \delta) \frac{V_d^2}{2} \right\}$$

with $\delta = \frac{K_p}{2\sqrt{2\psi_B - V_b}}$

Appendix B

If only two terms of the Taylor expansion of $(V_d + 2\psi_B - V_b)^{3/2}$ are taken into account, the dependancy of the depletion charge of V_d is lost.
This term is originated by the depletion depth (Eq. [3.13])

$$d(y) = \sqrt{\frac{2\varepsilon_s[V(y) + 2\psi_B - V_b]}{qN_A}}$$

The charge in the depletion layer is given by

$$Q_{depl}(y) = q\,N_A\,d(y) = \sqrt{2\varepsilon_s q N_A}\,\sqrt{V(y) + 2\psi_B - V_b}$$

Taylor expansion of $\sqrt{V(y) + 2\psi_B - V_b}$ yields

$$\sqrt{V(y) + 2\psi_B - V_b} = \sqrt{2\psi_B - V_b} + \frac{V(y)}{4\sqrt{2\psi_B - V_b}} + \cdots$$

If only one term is taken into account, the depletion charge is independent of V(y),

$$Q_{depl} \approx q\,N_A\,d_p = \sqrt{2\varepsilon_s q N_A}\,\sqrt{2\psi_B - V_b}$$

The channel charge is given by

$$Q_n(y) = -[V_g - 2\psi_B - V(y)]C_{ox} + \sqrt{2\varepsilon_s q N_A}\,\sqrt{2\psi_B - V_b}$$

Substitution of this equation into Eq. [3.11] and integration from the source (y = 0 , V = 0) to the drain (y = L, V = V_d) yields

$$I_d = \frac{W\mu_n C_{ox}}{L}\left\{\left(V_g - 2\psi_B - \frac{\sqrt{2\varepsilon_s q N_A}}{C_{ox}}\sqrt{2\psi_B - V_b}\right)V_d - \frac{V_d^2}{2}\right\}$$

$$= \beta\left\{(V_g - V_t)V_d - \frac{V_d^2}{2}\right\}$$

In this approximated equation the depletion width is constant and equal to the depletion width in the situation with zero drain voltage.

Appendix C1

Substitution of Eq. [3.30] and Eq. [3.31] into [3.29] yields

$$I_d = W \mu_n \frac{dV(y)}{dy} C_{ox} [V_g - V_t - V(y)]$$

$$I_d = \beta L \, [V_g - V_t - V(y)] \frac{dV(y)}{dy}$$

$$[V_g - V_t - V(y)] \frac{dV(y)}{dy} = \frac{I_d}{\beta L}$$

The solution follows by separation of variables

$$[V_g - V_t - V(y)] \, dV(y) = \frac{I_d}{\beta L} dy$$

$$(V_g - V_t) V(y) - \frac{V^2(y)}{2} = \frac{I_d}{\beta L} y + const$$

$$V(y) = (V_g - V_t) - \sqrt{(V_g - V_t)^2 - \frac{2 I_d}{\beta} \cdot \frac{y}{L}}$$

which can be found under the condition V(0) = 0.
For the saturated region, with $I_d = \beta (V_g - V_t)^2 / 2$ the potential distribution is given by

$$V(y) = (V_g - V_t) \left[1 - \sqrt{1 - \frac{y}{L}} \right]$$

Appendix C2

If field dependent mobility is taken into account the drain current continuity equation is given by

$$I_d = W \frac{\mu_0}{1 + \frac{dV(y)}{dy}/E_c} \frac{dV(y)}{dy} C_{ox} \left(V_g - V_t - V(y)\right)$$

$$I_d = \frac{W \mu_0 E_c C_{ox}}{E_c / \frac{dV(y)}{dy} + 1} \left(V_g - V_t - V(y)\right)$$

$$\frac{I_d}{\beta'} \left[E_c / \frac{dV(y)}{dy} + 1 \right] = V_g - V_t - V(y)$$

with

$$\beta' = W \mu_0 E_c C_{ox} = W v_{sat} C_{ox}$$

$$\frac{I_d}{\beta'} E_c = \left[V_g - V_t - V(y) - \frac{I_d}{\beta'} \right] \frac{dV(y)}{dy}$$

This is the differential equation which describes the potential distribution. Separation of variables and integration yields

$$\frac{I_d}{\beta'} E_c y = \left(V_g - V_t - \frac{I_d}{\beta'}\right) V(y) - \frac{V^2(y)}{2} + C$$

where C is the integration constant.
With the boundary condition $V(y=0)=V_s=0$ it is seen that $C=0$. Solving the quadratic relation yields

$$V(y) = \left(V_g - V_t - \frac{I_d}{\beta'}\right) \pm \sqrt{\left(V_g - V_t - \frac{I_d}{\beta'}\right)^2 - 2 \frac{I_d}{\beta'} E_c y}$$

Substitution of the boundary condition shows that only the minus sign holds.

Appendix D1

The drain current for the first MOST in the triode region must be equal to the drain current for the second MOST in the pentode region.

$$E_cL_2 + V_g' + \Delta V_t - V_{c2} - E_cL_2\sqrt{1 + 2\,\frac{V_g' + \Delta V_t - V_{c2}}{E_cL_2}} = \frac{V_g'V_{c2} - \frac{V_{c2}^2}{2}}{E_cL_1 + V_{c2}}$$

$$E_cL_1\left\{E_cL_2 + V_g' + \Delta V_t\right\} + V_{c2}\left\{E_cL_2 - E_cL_1 + \Delta V_t\right\} - \frac{V_{c2}^2}{2}$$

$$- \left(E_cL_1 + V_{c2}\right)E_cL_2\sqrt{1 + 2\,\frac{V_g' + \Delta V_t - V_{c2}}{E_cL_2}} = 0$$

In this equation the second power as well as the square root of V_{c2} exists. To solve this equation the following approximation will be made.

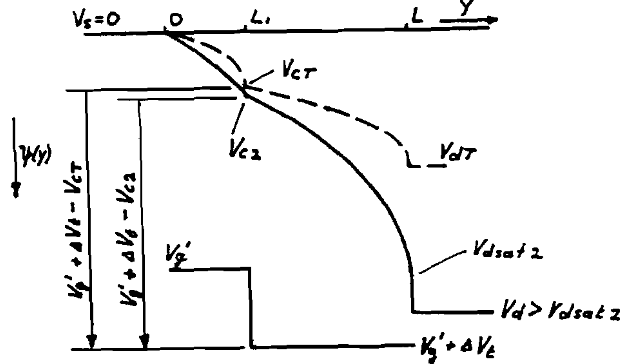

Comparison of the common voltage for the transition situation (dashed curve) and the common voltage for the TP-mode (solid curve) at large gate voltage.

If one replaces V_{c2} in the square root term by V_{cT}, which is a fixed value, the solution can be obtained by solving the quadratic equation.
The square root is approximated by :

$$E_cL_2\sqrt{1 + 2\,\frac{V_g' + \Delta V_t - V_{c2}}{E_cL_2}} \approx \sqrt{\left(E_cL_2\right)^2 + 2\,E_cL_2\left(V_g' + \Delta V_t - V_{cT}\right)}$$

By keeping in mind that

$$V_{cT} = \Delta V_t \sqrt{\frac{E_c L_1}{E_c L_2}}$$

$$V'_{gT} = \frac{(\Delta V_t)^2}{2 E_c L_2} + \Delta V_t \sqrt{\frac{E_c L_1}{E_c L_2}}$$

this can be written as

$$\sqrt{(E_c L_2)^2 + 2 E_c L_2 (V_g' - V'_{gT} + \Delta V_t) + (\Delta V_t)^2}$$

$$\text{or} \quad \sqrt{(E_c L_2 + \Delta V_t)^2 + 2 E_c L_2 (V_g' - V'_{gT})}$$

If $V'_g \longrightarrow V'_{gT}$ than $V_{c2} \longrightarrow V_{cT}$ and the error gets near zero. For large V_g' the error is negligible because the difference between $V'_g + \Delta V_t - V_{cT}$ and $V'_g + \Delta V_t - V_{c2}$ is relatively very small. (see fig.)
Which sign must be used in the solution of the quadratic relation follows by setting V'_g to V'_{gT} which must result in $V_{c2} = V_{cT}$.

Appendix D2

To derive the transconductance in the TP mode, the deravative

$$\frac{\partial V_{c2}}{\partial V_g'} \quad \text{is needed.}$$

This deravitive must not be obtained from the approximated solution given by Eq. [4.17], but has to be derived from the exact fourth power equation in Appendix D1. It can be obtained by implicit differentiation to V_g of this equation.

$$E_cL_1 + \frac{\partial V_{c2}}{\partial V_g'}\left\{E_cL_2 - E_cL_1 + \Delta V_t\right\} - \frac{\partial V_{c2}}{\partial V_g'} V_{c2}$$

$$- \frac{\partial V_{c2}}{\partial V_g'} E_cL_2 \sqrt{1 + 2\frac{V_g' + \Delta V_t - V_{c2}}{E_cL_2}} - (E_cL_1 + V_{c2}) \frac{1 - \frac{\partial V_{c2}}{\partial V_g'}}{\sqrt{1 + 2\frac{V_g' + \Delta V_t - V_{c2}}{E_cL_2}}} = 0$$

Appendix E

$$\alpha = \frac{K_{pn}^2}{K_n^2}$$

$$\beta = K_{pn}\left(1 + 2\frac{q\,d\,N_D}{C_{ox}K_n^2}\right) \implies \frac{q\,d\,N_D}{C_{ox}} = \frac{K_n^2}{2}\left(\frac{\beta}{K_{pn}} - 1\right)$$

$$\gamma = \frac{q\,d\,N_D}{C_{ox}}\left(1 + \frac{q\,d\,N_D}{C_{ox}K_n^2}\right)$$

$$\gamma = \frac{K_n^2}{2}\left(\frac{\beta}{K_{pn}} - 1\right)\left(1 + \frac{1}{2}\left(\frac{\beta}{K_{pn}} - 1\right)\right)$$

$$= \frac{K_n^2}{4}\left(\frac{\beta}{K_{pn}} - 1\right)\left(\frac{\beta}{K_{pn}} + 1\right)$$

$$= \frac{K_n^2}{4}\left(\frac{\beta^2}{K_{pn}^2} - 1\right)$$

$$= \frac{K_n^2}{4}\left(\frac{\beta^2}{\alpha K_n^2} - 1\right)$$

$$K_n^2 = \frac{\beta^2}{\alpha} - 4\gamma$$

$$K_{pn}^2 = \alpha K_n^2 = \beta^2 - 4\gamma\alpha$$

$$\frac{q\,d\,N_D}{C_{ox}K_{pn}} = \frac{\beta}{2\alpha}\left(1 - \sqrt{1 - 4\frac{\gamma\alpha}{\beta^2}}\right)$$